TITLE

Novel therapy for gastric cancer peritoneal dissemination using genetically modified dental pulp cells and astatine-211

AUTHORS

Koumei Kuge[1,2], Wan-Ying Du[1], Hiroki Masuda[1,2], Tomohiko Yasuda[1,2], Toshifumi Tatsumi[3], Xiaojie Yin[4], Masao Yoshino[5], Akira Sugiyama[6], Ryohei Numata[7], Wataru Yokoyama[7], Hidenori Shibahara[7], Tomoko Tanaka[3], Mika Kobayashi[3], Akashi Taguchi[3], Takahide Kohro[8], Naoko Takubo[3], Masahiro Nakamura[3], Jaewoong Jang[3], Yoshitaka Kumakura[3,9], Hiroshi Yoshida[2], Akira Yoshikawa[5,10], Hiromitsu Haba[4], Youichiro Wada[3]*, Kiwamu Imagawa[7]**, and Sachiyo Nomura[1,3,6]***

CORRESPONDENCE

*Co-corresponding author. Email: wada-y@ric.u-tokyo.ac.jp

** Co-corresponding author. Email: imagawa-k@jp.jcrpharm.com

*** Co-corresponding author. Email: sachiyo.nomura1012@gmail.com

AFFILIATIONS

19 [1] Department of Gastrointestinal Surgery, Graduate School of Medicine, The University of Tokyo

20 [2]Department of Surgery, Graduate School of Medicine, Nippon University

21 [3]Isotope Science Center, The University of Tokyo

22 [4]Nishina Center for Accelerator-Based Science, RIKEN

23 [5]Institute for Materials Research, Tohoku University

24 [6]School of Pharmacy and Pharmaceutical Sciences, Hoshi University Clinical Pharmaceutical

25 Sciences

26 [7]Regenerative Medicine Unit, Drug Discovery Research Institute, Research Division, JCR

27 Pharmaceuticals Co., Ltd.

28 [8]Department of Cerebrovascular Medicine, Jichi Medical School

29 [9]Department of Diagnostic Radiology and Nuclear Medicine, Saitama Medical Center, Saitama

30 Medical University

31 [10]New Industry Creation Hatchery Center, Tohoku University

32

33 **SUMMARY**

34 Peritoneal dissemination of gastric cancer represents a terminal stage with limited therapeutic

35 options and a five-year survival rate below 10%. To develop a more effective treatment, we

36 established a novel α-particle–based approach using genetically engineered human dental pulp

stem cells (DPCs) expressing the sodium/iodide symporter (NIS) to deliver astatine-211 (At-211) directly to tumor sites. DPCs, isolated and expanded under differentiation-suppressive conditions, showed strong tumor-homing ability when injected intraperitoneally into a mouse model of gastric cancer dissemination. Fluorescent imaging and histological analysis confirmed selective accumulation of DPCs within tumor lesions through CXCR4/SDF-1–mediated chemotaxis. Introduction of the NIS gene markedly increased SLC5A5 expression and enabled efficient uptake of At-211. High-resolution α-particle imaging visualized α-ray emission specifically from NIS-DPCs, confirming intracellular retention of the radionuclide. *In vivo*, sequential administration of NIS-DPCs followed by Na[At-211] led to pronounced regression of peritoneal tumors and significant survival extension compared with controls. The therapeutic mechanism involves three coordinated steps: tumor-directed migration of NIS-DPCs, At-211 uptake via NIS transporters, and localized α-particle–mediated cytotoxicity. This study introduces a novel concept of cell-based α-radiotherapy integrating regenerative and nuclear medicine. Given the established clinical safety of DPCs in humans (J-REPAIR, jRCT1080224505), this NIS-DPC platform offers a promising strategy for precise, short-range irradiation of disseminated gastric cancer and potentially other intractable malignancies.

INTRODUCTION

55 Peritoneal dissemination is a common terminal manifestation of gastric cancer and is
56 classified as stage IV disease, with a 5-year survival rate of less than 10%. Current therapeutic
57 options are largely palliative, highlighting an urgent need for new treatment strategies with
58 curative potential.

59 We previously established a murine gastric cancer peritoneal dissemination cell line
60 (YTN16) and demonstrated proof-of-concept efficacy of targeted α-particle therapy using
61 astatine-211 (At-211), a high–linear energy transfer radionuclide with a 7.2-hour half-life. An
62 anti–fibroblast growth factor receptor 4 (FGFR4) antibody—selected for its high expression on
63 YTN16 cells—was conjugated to At-211 via a halogen–tin exchange reaction. In vivo
64 biodistribution studies in a syngeneic C57BL/6J peritoneal dissemination model showed that
65 intraperitoneal administration achieved peak peritoneal radioactivity at 4.5 hours, resulting in
66 marked tumor regression and significant survival extension compared with untreated controls.

67 However, the therapeutic window is constrained by the mismatch between the time
68 required for antigen–antibody binding (~24 hours) and the physical half-life of At-211. To
69 improve delivery kinetics, we sought a vehicle capable of rapidly homing to the tumor
70 microenvironment. Tumors actively recruit stromal fibroblasts to form cancer-associated
71 fibroblasts (CAFs), and mesenchymal cells (MSCs) share similar tumor-tropic properties. We

72 therefore investigated dental pulp cells (DPCs) developed by JCR Pharmaceuticals, which have
73 an established manufacturing process and demonstrated safety in a phase 1/2 clinical trial for
74 acute ischemic stroke (Ref. jRCT1080224505).

75 Here, we evaluate DPCs as a biologic vector for targeted α-particle therapy in gastric
76 cancer peritoneal dissemination. We hypothesize that leveraging the tumor-homing ability of
77 DPCs can facilitate At-211 delivery to the tumor niche, overcoming the limitations of
78 radioimmunotherapy and enabling improved therapeutic efficacy and survival outcomes.

79

80

81

82 **RESULTS**

83 **Preparation and characteristics of DPCs**

84 Dental pulp cells are located in the dental pulp, the soft connective tissue found in the
85 center of teeth (Figure 1a). They play key roles in tooth vitality by producing dentin, supporting
86 sensory functions, and participating in immune defense and tissue repair (Ref. Nito).

87 Dental pulp extraction is followed by mild enzymatic digestion to loosen the
88 extracellular matrix, then mechanical mincing to produce small tissue pieces. These explants are
89 placed in culture, allowing maintenance and expansion of dental pulp cells (DPCs) (Ref.
90 Gronthos) (Figure 1b).

91 DPCs could be expanded using culture medium, but no proliferation was observable in
92 soft agar, suggesting no tumorigenicity after injecting *in vivo* (Figure 1c).

93

94 **Confirmation of DPC accumulation in peritoneal tumor tissue**

95 To investigate that DPCs harbor the ability of tumor accumulation, we applied them into
96 the peritoneal cavity of gastric cancer dissemination model, which was established previously by
97 us (Ref.Yamamoto). Firstly, 5 x10^5 cells of DPCs were prepared as described in materials and
98 methods. Then they were labeled with fluorescence dye (DiR) for living cells. After 24 hours,
99 injected mouse models were euthanized, and peritoneal surface was opened to apply florescence

100 detection camera. Localization of injected DPCs was visualized using in vivo imaging system
101 (IVIS Lumina III), and compared with distribution of disseminated visible lesions. As shown in
102 Figure 2, lesion occupied area was surrounded by blue line (right in Figure 2a, left in 2b).
103 Fluorescent images obtained by fluorescent camera was shown in Figure 2c (left) and 2d (right).
104 Significant colocalization was observable in both sides, suggesting accumulation of DPCs to
105 gastric cancer cells.

106 To further evaluate the specificity of tumor-directed accumulation, 1.0×10^6 DPCs were
107 injected intraperitoneally into a gastric cancer mouse model. Two days after the last injection of
108 DPCs, mice were sacrificed, and peritoneal tissues were fixed and subjected to
109 immunohistochemical staining using an anti-human Lamin B1 antibody. Brown staining,
110 indicative of DPC localization, was observed in tissues surrounding established tumor lesions
111 (Figure 2e, f), whereas no staining was detected in tissues lacking tumor cell engraftment (Figure
112 2g). These findings strongly suggest that intraperitoneally administered DPCs migrate to and
113 accumulate within peritoneal dissemination sites.

114 To validate the migratory ability of the DPCs towards the YTN16 cell line, a migration
115 assay was performed using a Transwell chamber. After $1x10^5$ DPCs were placed in the upper
116 chamber, a series of different numbers of YTN16 cells were placed in the lower chamber. The
117 migrated cells on the other side of the micropore membrane were stained with a Calcein solution,

118 and the absorbance was measured. Figure 2h shows that the presence of YTN16 cells induces
119 DPC migration in a cell number-dependent manner and proves the migration capability of DPCs
120 to YTN16 cells.
121
122 **Functional transduction of NIS to DPC**
123 The sodium-iodide symporter (NIS) is a transmembrane glycoprotein with 13
124 transmembrane domains that transports radioactive isotopes, such as I-131, I-123, I-125, I-124,
125 Tc-99m, Re-188, and At-211, into cells (Ref. Darrouzet). Therefore, we introduced the NIS gene
126 (SLC5A5) into DPC cells using lentivirus (Figure 3a). While there was no change in the
127 expression levels of other NIS-encoding genes, such as SLC26A4 and SLC26A7, the expression
128 level of SLC5A5 in NIS-DPC increased more than 100-fold.
129 Next, we verified the expression level of NIS molecules on the cell surface and
130 evaluated the correlation between uptake capacity and positive rate using iodine as a surrogate
131 molecule in vitro. The results are shown in Figure 3b and 3c. We confirmed that iodine uptake
132 increased in a NIS-positive rate-dependent manner and observed a trend where higher NIS-
133 positive rates correlated with higher iodine uptake (Figure 3c). When iodine uptake was
134 confirmed in three lots of NIS-DPC cells, more iodine uptake was observed compared to DPC

135 cells without gene introduction. This confirmed that the introduced NIS gene was expressed on

136 the cell surface and that its function was maintained (Figure 3b).

137 To validate that NIS-DPCs could migrate to dissemination lesions, NIS-DPCs were

138 injected into the peritoneal cavity, as was done with DPCs. Two days after injection, the peritoneal

139 tissues were subjected to immunohistochemical staining using an anti-human lamin B1 antibody.

140 As shown in Figure 2e and 2f, brown staining indicative of NIS-DPC localization was observed

141 in tissues surrounding established tumor lesions (Figures 3d and 3e), whereas no staining was

142 detected in tissues lacking tumor cell engraftment (Figure 3f). These findings strongly suggest

143 that the NIS-DPCs administered intraperitoneally were able to accumulate within peritoneal

144 dissemination lesions.

145

146 **Uptake of At-211 by NIS-DPC**

147 Recently, it has been reported that, due to its various chemical forms, purified At-211

148 undergoes nonspecific binding in vivo, and that this can be controlled by converting it to sodium

149 astatine-211 (Ref. Watabe 2022). Therefore, prior to in vivo administration, we prepared sodium

150 astatine-211 using the method shown in Figure 4a. We confirmed that the purified At -211 had a

151 uniform chemical form using thin layer chromatography (TLC) (Figure 4b).

Furthermore, we confirmed the amount of At-211 that was taken up by the cells. The results are shown in Figure 4c. As with the results of the confirmation of uptake capacity using a surrogate molecule, NIS-DPC cells with the introduced NIS gene took up more At-211 than DPC cells without the introduced gene. Additionally, the highest uptake was observed at 5 minutes when comparing changes in uptake amount over time at 5, 10, and 60 minutes after At-211 addition. These results suggest that At-211 is rapidly taken up by DPC cells via NIS. Therefore, pre-accumulating NIS-DPC cells around the peritoneal dissemination site and then administering At-211 allows the drug to be taken up by cells quickly enough to be effective within its half-life.

Novel contact scintillator imaging of alpha-ray trajectories from alpha emitters

Because the NIS-DPC cell fraction is radioactive, the uptake of At-211 was suggested. However, to verify that the alpha rays emitted from At-211 originate from the NIS-DPC cells, a camera that can visualize alpha rays on a 1 μm scale was used. Figure 5a shows the alpha camera system configuration (Ref. Yamamoto 2023) (Ref. Yoshino 2025). It comprises three principal components: (i) a 100-μm-thick GAGG thin-film scintillator screen; (ii) an infinity-corrected magnification optical train consisting of an objective, an imaging lens; and (iii) a CMOS imaging sensor, specifically the ORCA-Quest 2 qCMOS (C15550-22UP) from

170 Hamamatsu Photonics. Alpha particles emitted from within the cells are converted into photons
171 by a GAGG scintillator, magnified by a 20x objective, and detected by a CMOS sensor. Figure
172 5b shows an overview of the system. Eighteen thousand NIS-DPC and DPC cells were cultured
173 in an eight-well chamber slide. Then, 500 kBq of At-211 was added to the culture medium per
174 well, followed by a 30-minute incubation period. The cells were then fixed with formalin, and
175 observation with an alpha camera was conducted for ten minutes. Figure 5c shows an overview
176 of the NIS-DPC cells and Figure 5f shows an overview of the DPC cells. Both exhibit similar
177 morphology and distribution. However, as Figures 5d and 5g show, the alpha particle range was
178 detected only in the NIS-DPC cells. The merged image in Figure 5h confirms localization in the
179 NIS-DPC cells. These results indicate that At-211 was efficiently taken up by NIS-DPC cells
180 and that α-rays were emitted from these cells.
181
182 **At-211 and NIS-DPC cell administration showed antitumor effects**
183 Then, we preliminarily assessed the antitumor and survival prolongation effects of At-
184 211 and NIS-DPC administration in a mouse peritoneal dissemination model. Three weeks after
185 tumor cell transplantation, 0.5×10^6 NIS-DPC cells were administered intraperitoneally.
186 Twenty-four hours later, 0.6 MBq of astatine-211 was administered per animal. At one and a
187 half weeks post-transplantation, examination of the peritoneum revealed tumor cells in the

188 peritoneal dissemination group (Figure 6a), as well as in the NIS-DPC administration group
189 (Figure 6b) and the astatine-211 administration group (Figure 6c). However, the disappearance
190 of peritoneal seeding was observed in the group that received both NIS-DPC and astatine-211
191 (Figure 6d, asterisks).

192 To evaluate the effect of NIS-DPC&At-211 treatment, we scored the antitumor effects
193 visually on a 5-point scale (0–4) based on the extent of cancer cells adhering to the peritoneal
194 tissue at the time of death or at the end of the observation period (Figure 6e). We then evaluated
195 the results using the Tukey test.

196 The results of the antitumor effect evaluation are shown in a box-and-whisker plot
197 (Figure 6f). Compared to the untreated group (No Treatment) and the At-211 monotherapy
198 group (At-211), a significant reduction in score (i.e., reduction in disseminated tissue) was
199 observed in the At-211+NIS-DPC group (At-211+NIS-DPC). It was therefore suggested that the
200 administered NIS-DPC accumulated around implanted cancer cells in the peritoneum.
201 Subsequently, the cancer tissue was reduced by the cytolytic effect of α-rays after the uptake of
202 the administered At-211.

203 Using the same evaluation scale, we performed a series of experiments to optimize the
204 radioactivity of At-211 (Figure S6a), dose of NIS-DPC (Figure S6b), and repetition of NIS-DPC
205 injection (Figure S6c). Based on the macroscopic evaluation of the extent of peritoneal

206 dissemination, 0.6MBq of At-211/body, $5x10^5$/body of NIS-DPC, three-time administration of

207 NIS-DPC, provided significantly higher score.

208 Using this optimized regimen, survival rates were evaluated using Kaplan-Meier

209 curves and Logrank tests. The survival rates of individual mice in each group after At-211

210 administration were evaluated. The results are shown in Figure 6g. Compared to the untreated

211 group and the At-211 treated group, a significant prolongation of survival was observed in the

212 At-211 + NIS-DPC group. Based on these results, the extension of the survival rate is

213 considered to be due to the damage and reduction of the implanted tumors by At-211 and NIS-

214 DPC in the mouse peritoneal dissemination model.

215

216

DISCUSSION

Brief summary

In this study, we created NIS-DPC cells by forcing the expression of the NIS gene, which encodes an iodine transporter, in DPC cells that accumulate in the peritoneal cavity. Forty-eight hours after administering these cells, we introduced astatine-211 into the peritoneal cavity, demonstrating that the NIS-DPC cells accumulated around the tumor cells were rapidly taken up, resulting in tumor cell death. This three-step treatment method is illustrated in Figure 7: addition of NIS-DPC cells, addition of At-211, and α-ray irradiation. The first process involves the accumulation of NIS-DPC cells in tumors. The second process involves the uptake of astatine-211 by NIS-DPC cells. The third process involves tumor-killing effects.

Accumulation of DPC/NIS-DPC to cancer cells

It is known that cancer cells accumulate large numbers of cancer-associated fibroblasts (CAFs) in their vicinity. However, mesenchymal stem cells (MSCs) exhibit similar dynamics to CAFs. MSCs migrate in response to chemokines, such as SDF-1, produced by cancer cells. They recognize these chemokines via CXCR4. However, due to protein cross-reactivity between humans and mice, human MSCs can migrate toward mouse tumors as well. Additionally, MSCs have low immunogenicity and can be administered allogeneically. Since 2008, when it was

235 reported that DPC cells (a type of MSC) express CXCR4 and migrate in response to SDF-1 (Ref.
236 Jiang 2008), it has frequently been reported that DPC cells accumulate in inflammatory or
237 ischemic sites, particularly in oral and maxillofacial surgery (Ref. Yamaguchi et al., Sci. Rep.
238 2015) (Ref. Li et al., Sci. Rep. 2017)(Ref. Neves et al., Sci. Rep. 2020)(Ref. Kornsuthisopon et
239 al., Sci. Rep. 2022) (Ref. Irfan et al., Sci. Rep. 2023). DPCs produced by JCR Pharmaceuticals,
240 which have been administered to humans and proven safe (Ref. Suda 2022), were examined for
241 their ability to migrate and accumulate around tumor tissues in a mouse peritoneal dissemination
242 model.

243 As mentioned above, the first process of this therapy is accumulation of DPC cells to
244 cancer cells. To prove this, multimodal experiments were performed. Macroscopically, as shown
245 in Figures 2a to 2d, the localization of fluorescently labeled DPC cells coincided with the
246 localization of gastric cancer peritoneal dissemination lesions. Microscopically, as shown in
247 Figures 2e to 2g, DPC cells were observed within gastric cancer lesions via immunohistochemical
248 staining. These findings indicate that DPC cells accumulate in tumor cells.

249 In vitro, DPC cells were observed migrating toward gastric cancer cells (Figure 2h).
250 However, the molecular mechanism underlying this migration is suggested to involve the
251 induction of EGR1 in DPC cells by soluble factors released from cancer cells. Further clarification
252 of the migration mechanism is needed in further study.

253

254 **Functional uptake of At-211 by NIS-DPC**

255 The second step of this treatment method involves the uptake of At-211 by DPC cells.
256 Several experiments were conducted to determine if the introduced iodine transporter functions
257 in DPC cells. First, non-radioactive iodine and a non-radioactive ligand were added to DPC cells
258 expressing NIS, and the uptake efficiency was examined. As Figures 3b and 3c show, DPC cells
259 expressing NIS exhibited approximately 50-fold higher iodine uptake. The amount of uptake
260 increased in a NIS expression-dependent manner, demonstrating that NIS functionally takes up
261 the ligand. Furthermore, Figure 4c shows efficient uptake of At-211 by NIS-DPC starting five
262 minutes after At-211 addition. Using the newly developed α camera, we confirmed that the uptake
263 of At-211 and cell localization were consistent. This indicates that NIS-DPC cells take At-211
264 into the cell and emit α rays. In the future, it is expected that the lethal effect of α rays on tumor
265 cells will be directly visualized by co-culturing NIS-DPC cells with tumor cells and observing
266 them using the α camera.

267

268 **Tumoricidal effect of NIS-DPC&At-211**

269 As shown in Figure 6, this study demonstrated that administering At-211 after NIS-DPC
270 administration reduced peritoneal dissemination lesions and prolonged survival. This confirms

271 the tumor-killing effect, which is the third process in this treatment. In the evaluation of anticancer
272 drug efficacy in humans, the primary endpoint is survival rate extension. Therefore, when
273 evaluating the efficacy of cancer treatments using model animals, improvement in survival rate is
274 equally important as it is in humans. Furthermore, the proposed mechanism of action was strongly
275 implicated. However, it has been reported that immune function induced by neoantigens released
276 from tumor cells damaged by radiation exposure contributes to the efficacy of nuclear medicine
277 therapy (Ref. Nagaoka). Elucidating the detailed mechanism in the future may expand the
278 application of combined therapy with NIS-DPC cells and astatine-211.
279
280 **Requirement for practical application**
281 To commercialize this treatment method in the future, data on its efficacy must be
282 accumulated. Additionally, data on the safety and pharmacokinetics of the reagents used in this
283 study will be necessary. Since DPC cells have been administered to humans before and their safety
284 has been demonstrated (Ref. Suda 2022), data on the safety of NIS-DPC is necessary. In particular,
285 since lentiviruses are used to introduce the NIS gene, it is necessary to clarify whether they are
286 excreted from the administered animals. Furthermore, since astatine-211 is administered in the
287 form of sodium astatine into the abdominal cavity, pharmacokinetic data must be obtained in
288 medium-sized animals prior to human administration. Human clinical studies will be conducted

289 based on these data.

290 DPC cells can be administered allogenically. Since their procurement is minimally
291 invasive, the cells can be stored frozen, which makes it feasible to establish a supply system.
292 Additionally, meeting clinical demand for At-211 is possible through the future widespread
293 adoption of mass production technology and the development of dedicated accelerators.

294

295 **Perspective**

296 Here, we reported a new treatment method combining nuclear and regenerative
297 medicine products. Since the safety of DPC cells has already been proven in humans, a first-in-
298 human trial should be conducted after the safety of NIS-DPC and At-211 is evaluated.

299

300

301

302

303

304 **MATERIALS AND METHODS**

305 **Preparation of Dental Pulp Cells (DPCs)**

306 Human dental pulp cells (DPCs) were isolated from extracted teeth under sterile
307 conditions, as previously described with minor modifications. Briefly, extracted teeth were first
308 disinfected by immersion in 1% formalin solution followed by washing with sterile physiological
309 saline to remove debris and surface contaminants.

310 The tooth structure was mechanically fractured using a dental rongeur, and the pulp
311 tissue was carefully extracted from the pulp chamber. The obtained pulp tissue was minced into
312 small fragments using sterile surgical scissors and transferred into a tube containing Liberase
313 digestion solution (Roche Diagnostics, Basel, Switzerland). The tissue suspension was incubated
314 at 37°C for enzymatic digestion with gentle agitation until the connective matrix was adequately
315 loosened.

316 After digestion, the suspension was mixed with Dulbecco's Modified Eagle Medium
317 (DMEM) supplemented with 10% fetal bovine serum (FBS) and 1% penicillin/streptomycin (P/S)
318 to terminate the enzymatic reaction. The mixture was centrifuged at 300 × g for 5 min, and the
319 supernatant was discarded. The resulting pellet was resuspended in fresh DMEM containing 10%
320 FBS and 1% P/S and seeded onto tissue culture plates.

321 Cells were incubated at 37°C in a humidified 5% CO_2 atmosphere and expanded until

322 passage 5 (P5). From passage 1 (P1) onward, cultures were maintained in DMEM supplemented
323 with 10% FBS but without antibiotics, to avoid potential effects of antimicrobial agents on cell
324 proliferation or differentiation. All procedures were conducted under aseptic conditions using
325 biosafety level 2 (BSL-2) practices.
326
327 **Soft Agar Colony Formation Assay**
328 To evaluate anchorage-independent growth and confirm the non-transformed
329 characteristics of the cells, a soft agar colony formation assay was performed using the
330 CytoSelect™ 96-Well Cell Transformation Assay Kit (Cell Biolabs, Inc., San Diego, CA, USA),
331 according to the manufacturer's protocol.
332 HeLa, DPC, and NIS-DPC cells were cultured under standard conditions until reaching
333 logarithmic growth phase. Cells were then harvested and resuspended in assay medium at the
334 following densities: 8×10^3 cells/well for HeLa, and 8×10^4 cells/well for DPC and NIS-DPC.
335 Cell suspensions were seeded in duplicate 96-well soft agar plates (Plate ① and Plate ②) as
336 described in the kit instructions.
337 Plate ① was incubated for 7 days at 37°C in a humidified 5% CO_2 incubator to allow
338 potential colony formation. Plate ② was processed immediately after cell seeding for background
339 measurement following the manufacturer's procedures: agar dissolution, cell lysis, and nuclear

340 staining. The absorbance of each well was measured using a microplate reader to determine
341 baseline optical density (OD).
342 After the 7-day incubation period, Plate ① was subjected to the same lysis and staining
343 procedures, and absorbance was measured again. Colony formation was quantified by comparing
344 OD values between the 0-day (Plate ②) and 7-day (Plate ①) samples. As expected, a significant
345 increase in OD was observed only in the HeLa group, while DPC and NIS-DPC cells showed no
346 increase, confirming their non-transformed phenotype.
347
348 **Preparation of mouse model and application of NIS-DPC followed by Na[At-211]**
349 Six-week-old female C57BL/6J mice were purchased from Jackson Laboratoy Japan
350 and housed in a specific pathogen-free environment at the Animal Experiment Facility in
351 Isotope Science Center, the University of Tokyo. The animal use proposal and experimental
352 protocol were reviewed and approved by the University of Tokyo Animal Committee (ID: Med-
353 P22-084、A2024ISC003). The YTN16 cell line was maintained in Dulbecco's modified
354 Eagle's medium (DMEM, Sigma-Aldrich Merck, Tokyo, Japan) with 10% heat-inactivated fetal
355 bovine serum (FBS, BWT, France), 50 μg/mL streptomycin, 50 U/mL penicillin
356 (ThermoFisher, Tokyo, Japan), and MITO + serum extender (Corning, Corning, NY, USA). A
357 total of 1×10^7 YTN16 cells were suspended in 500 μL of Hanks' Balanced Salt Solution and

358 intraperitoneally injected into mice (Ref. Nagaoka). Starting the following day, 2 μg of

359 thyroxine was administered orally once daily. At 8, 10, and 12 days after YTN16 cell injection,

360 1×10^6 NIS-DPC cells, 1×10^6 DPC cells, or vehicle alone were administered intraperitoneally.

361 On day 14, Na[At-211] (0.6 MBq) dissolved in 0.5 mL of vehicle was injected intraperitoneally.

362 On day 35 after YTN16 cell injection, the peritoneal cavity was examined, or the mice were

363 observed until death or humane sacrifice, followed by examination of the peritoneal cavity.

364

365 **Construction of Lentiviral Vector pLVSIN-EF1α-hNIS-Pur**

366 A self-inactivating (SIN) lentiviral expression vector, pLVSIN-EF1α-hNIS-Pur, was

367 constructed based on the parental plasmid pLVSIN-EF1α-Pur (Takara Bio Inc.). The human

368 sodium/iodide symporter (hNIS) gene (sequence ID No. 2; NCBI accession number

369 NM_000453.3) was inserted into the multiple cloning site of the parental vector.

370 The DNA fragment encoding hNIS was synthesized with a Not I site at the 5′ end and a BamH I

371 site at the 3′ end. Both the hNIS insert and the pLVSIN-EF1α-Pur vector were digested with the

372 respective restriction enzymes Not I and BamH I (New England Biolabs or equivalent) to

373 generate compatible cohesive ends. The digested fragments were ligated using Ligation High

374 Ver. 2 (TOYOBO Co., Ltd.), yielding the recombinant plasmid pLVSIN-EF1α-hNIS-Pur.

375 All recombinant DNA manipulations were carried out under standard molecular cloning

376 conditions in accordance with institutional biosafety regulations.

377

378 **Lentiviral Packaging and Production**

379 Lentiviral particles carrying the pLVSIN-EF1α-hNIS-Pur construct were produced
380 using a self-inactivating lentiviral packaging system. In addition to the expression vector
381 described above, a mixture of packaging plasmids encoding HIV-1–derived structural and
382 regulatory proteins (Gag, Pol, Tat, and Rev) and the vesicular stomatitis virus G glycoprotein
383 (VSV-G) envelope was provided by the Lentiviral High Titer Packaging Mix (Takara Bio Inc.).
384 Viral particles were generated following a modified standard protocol.

385 Poly-L-lysine–coated culture dishes were seeded with cells at a density of
386 approximately 5×10^4 cells/cm² and incubated overnight at 37°C in a humidified 5% CO_2
387 incubator. On the following day, a DNA mixture was prepared by adding 7 μL of Packaging Mix
388 and 11 μL of pLVSIN-EF1α-hNIS-Pur plasmid DNA (0.5 μg/μL) to 1.5 mL of Opti-MEM I
389 Reduced Serum Medium (Gibco).

390 Transfection was performed using either FuGENE HD (Promega) or TransIT-Lenti Transfection
391 Reagent (Takara Bio Inc.), according to the manufacturers' instructions. The transfected cells
392 were incubated at 37°C in 5% CO_2 for approximately 24 hours, after which the culture supernatant
393 was replaced with 10 mL of DMEM (Gibco) and incubation continued for another 24 hours.

394 The culture supernatant containing lentiviral particles was collected and clarified by
395 centrifugation at 500 × g for 10 minutes. The supernatant was then passed through a 0.45 μm filter
396 (Millipore, Cat. No. SLHPR33RB) to remove cellular debris. The filtered viral solution was
397 aliquoted into microtubes and stored at −80°C until use.
398
399 **Generation of hNIS-Expressing Dermal Papilla Cells (hNIS-DPCs)**
400 Dental pulp cells (DPCs) were seeded at a density of 2.0×10^4 cells/cm² and cultured
401 overnight at 37°C in a humidified 5% CO_2 incubator. On the following day, cells were transduced
402 with the hNIS lentiviral vector (hNIS-LV) at a multiplicity of infection (MOI) of 10. To enhance
403 viral transduction efficiency, protamine sulfate (Sigma-Aldrich, Cat. No. P4020) was added to
404 the viral inoculum at a final concentration of 100 μg/mL.
405 The viral supernatant was removed 24 hours after infection and replaced with fresh
406 DMEM (Gibco, Cat. No. 10567-014). Cells were cultured with medium changes every 2–3 days,
407 and cell morphology and confluence were monitored microscopically. When cultures reached
408 approximately 90% confluence, cells were passaged using standard trypsinization procedures.
409 For selection of transduced cells, puromycin was added to the culture medium at a final
410 concentration of 1 μg/mL during the first passage after viral infection. Resistant colonies were
411 expanded under puromycin selection. Thereafter, cells were maintained in standard DMEM

412 without selection antibiotic for one to two additional passages to establish a stable hNIS-DPC line.

413 Established cells were cryopreserved in liquid nitrogen for long-term storage.

414

415 **Cell Culture**

416 NIS-DPC and YTN16 cells were cultured in Dulbecco's modified Eagle's medium

417 (DMEM; Gibco, Cat. No. 10567014) under standard conditions (37°C, 5% CO_2). Cells were

418 maintained for 3 to 4 days before use.

419

420 **Cell Harvesting and Co-culture Setup**

421 Cells were detached using 0.25% trypsin–EDTA (Gibco, Cat. No. 25200056) and

422 resuspended in fresh DMEM. Cell concentrations were adjusted to 1×10^5 cells/mL. For co-

423 culture experiments, cells were seeded into 24-well Transwell plates (Corning, Cat. No. 353504)

424 equipped with cell culture inserts (Corning, Cat. No. 351152). NIS-DPC cells (1×10^5 cells) were

425 seeded in the upper insert, and YTN16 cells (1×10^5 cells) were seeded in the lower chamber. The

426 co-cultures were incubated for 48 hours at 37°C in a humidified incubator with 5% CO_2.

427

428 **Migration assay**

429 After 48 hours of co-culture, the medium was aspirated and replaced with DMEM

430 containing 1% human serum albumin (HSA) prepared from 25% clinical-grade albumin solution
431 (Takeda Pharmaceutical Co., Ltd.). Cells were stained with Calcein (Dojindo, Cat. No. 341-
432 07901) according to the manufacturer's instructions to visualize viable cells. Fluorescence
433 intensity was quantified using a spectrophotometric plate reader, and fluorescent images were
434 captured using a fluorescence microscope under identical exposure conditions for all samples.

435

436 **Cell Labeling with DiR and In Vivo Administration**

437 NIS-DPC cells were suspended in medium at a concentration of 1×10^7 cells/mL. The
438 cell suspension was mixed with an equal volume of 20 μmol/L DiR dye solution (Thermo
439 Fisher Scientific or equivalent), resulting in a final dye concentration of 10 μmol/L. The mixture
440 was incubated for 15 minutes at room temperature in the dark, with gentle tapping every 5
441 minutes to ensure homogeneous labeling. After incubation, the cells were washed three times
442 with injection medium by centrifugation to remove excess dye. The labeled cells were
443 resuspended in injection medium at a final concentration of 1×10^6 cells/mL. Labeled NIS-DPC
444 cells were administered intraperitoneally to peritoneal dissemination model mice. All animal
445 experiments were conducted in accordance with institutional guidelines and approved by the
446 relevant Animal Care and Use Committee.

447

448 **In Vivo Fluorescence Imaging**

449 At predetermined time points after injection, mice were sacrificed, and peritoneal
450 tissues were harvested. DiR fluorescence signals were detected using an in vivo imaging system
451 (IVIS Lumina III; PerkinElmer) under the following parameters: excitation filter, 740 nm;
452 emission filter, 790 nm; and exposure time, automatic setting. Fluorescence images were
453 analyzed using the manufacturer's software.

454

455 **Production of ^{211}At**

456 According to the procedure described in Refs. (Yin 2023, Yin 2024), the radioisotope of
457 At-211 was produced in the nuclear reaction of ^{209}Bi(α,2n)^{211}At using the AVF cyclotron of the
458 RIKEN RI Beam Factory.

459

460 **Ppreparation of Na[At-211]**

461 Dry solid At-211 of multiple chemical species in glass vial was dissolved the injection
462 water (100 μL). At-211 aqueous solution (63 MBq, 50 μL) was mixed with 1% ascorbic acid,
463 2.3% MEYLON Injection aqueous solution (1 mL). After stirreing briefly, the reaction solution

464 of At-211 was left to stand for 1hour at room temperature under sealed condition to afford the
465 Na[At-211]. The Na[At-211] solution was dissolved 1% ascorbic acid, 2.3% MEYLON Injection
466 aqueous solution, and used animal experiments and the cell tracer experiments.
467

468 **Thin-Layer Chromatography (TLC) Analysis**

469 Thin-layer chromatography (TLC) was performed using silica gel 60 plates (Merck) as
470 the stationary phase. Samples (5 μL, 280 kBq) were spotted onto the plate and developed in a
471 solvent system consisting of acetonitrile and Milli-Q water (CH_3CN:MQ = 2:1, v/v).
472 After development, the chromatograms were analyzed using a TLC scanner (Scan-RAM;
473 LabLogic Systems Ltd.) equipped with a ZnS scintillation detector. Radioactivity on the TLC
474 plates was quantified using the manufacturer's analysis software.
475

476 **Quantitative measurement of At-211 uptake**

477 Na[At-211] (10 kBq) was added to the DPC and NIS DPC cell and incubated for 5
478 min, 30 min, and 1 h, respectively. After incubation, the medium was removed and the cells were
479 collected. The radioactivity of the samples was then measured with a γ-counter, and the counts
480 per minute (CPM) were calculated.
481

482 **Visualization of alpha-ray**

483 Alpha-particle track images were acquired with a CMOS sensor at 1-s exposure,
484 yielding 600 frames each for NIS-DPS and DPC cells. Image analysis was conducted in ImageJ
485 (v1.54f). For each frame, a fixed intensity threshold was applied, followed by morphological
486 operations to generate a binarized mask of suprathreshold regions. Each image was then
487 accumulated with its corresponding mask to isolate regions of interest surrounding the α-particle
488 tracks, and the resulting stacks were Z-projected to produce composite track images.

489

ACKNOWLEDGEMENTS

The radioisotope of At-211 was produced at the RI Beam Factory operated by the RIKEN Nishina Center and the CNS, University of Tokyo, Japan. The authors gratefully acknowledge Yousuke Kanayama, Nozomi Sato, Akihiro Nambu, Tomohiro Tomitsuka, Hiromichi Shimizu, Yudai Shigekawa, Sayantani Mitra, and Keiko Watanabe of RIKEN Nishina Center for technical assistance with the At-211 production.

FUNDING

This work was supported by Grants-in-Aid for Scientific Research (KAKENHI) from the Japan Society for the Promotion of Science (JSPS), including "Development of novel radiopharmaceuticals using α-emitting radionuclides and antibody drug delivery systems" (grant number 23H00419); "Collaborative research on therapeutic radionuclide production and radiopharmaceutical synthesis" (grant number 20KK0174); "Development of novel therapy for peritoneal dissemination using neoantigen activation induced by short-lived α-emitting radionuclides" (grant number 24K02393); "Experimental study of intraperitoneal radiotherapy for gastric cancer dissemination using highly selective short-lived α-particle delivery" (grant number 19H03510); and "Development of radiation imaging technology for detecting micro–peritoneal dissemination of gastric cancer" (grant number 21H00169).

Additional support was provided by the Uehara Memorial Foundation ("Development of radionuclide production technology and novel radiopharmaceuticals through accelerator science") and the Nakatani Foundation for Advancement of Measuring Technologies in Biomedical Engineering ("Development of theranostic technology using α-emitting radionuclides").

AUTHOR CONTRIBUTIONS

S.N. conceived and supervised the study and performed animal experiments. K.K., H.Y., H.M., T.Y., and W.-Y.D. conducted animal experiments. Y.W. performed α-particle therapy experiments and contributed to manuscript preparation. T.T. performed sodium astatide (At-211) synthesis. M.K. conducted cell culture experiments. A.T. performed RNA-seq data acquisition. T.Ta. analyzed pathological specimens. J.J. conducted At-211 compound analyses. Y.K. performed imaging studies. A.S. carried out α-particle uptake assays. R.N. prepared DPC cells. W.Y. performed functional analyses of DPCs. H.S. performed genetic modification of DPCs. K.I. managed DPC manufacturing and quality control. H.H. and X.Y. developed At-211 production technology. M.Yo. performed direct α-particle imaging. A.Yo. developed scintillators. T.K. and N.T. performed bioinformatics analyses. M.N. supervised bioinformatics and data integration. All authors discussed the results and approved the final manuscript.

COMPETING INTERESTS

N/A

DATA AND MATERIALS AVAILABILITY

under preparation

533 **REFERENCES**

534 A randomized, double-blind, placebo-controlled, multicenter study to evaluate the safety and
535 efficacy of JTR-161 in patients with acute ischemic stroke (jRCT1080224505).
536 **Japan Registry of Clinical Trials**, registered in 2022.
537

538 C. Nito, K. Sowa, M. Nakajima, Y. Sakamoto, S. Suda, Y. Nishiyama, A. Nakamura-Takahashi,
539 Y. Nitahara-Kasahara, M. Ueda, T. Okada, and K. Kimura, Transplantation of human dental pulp
540 stem cells ameliorates brain damage following acute cerebral ischemia. **Biomedicine &**
541 **Pharmacotherapy** 108, 1005–1014 (2018).
542

543 S. Gronthos, M. Mankani, J. Brahim, P. G. Robey, and S. Shi, Postnatal human dental pulp stem
544 cells (DPSCs) in vitro and in vivo. **Proceedings of the National Academy of Sciences of the**
545 **United States of America** 97, 13625–13630 (2000).
546

547 Y. Yamamoto, S. Nomura, A. Hosoi, K. Nagaoka, T. Iino, T. Yasuda, T. Saito, H. Matsushita, E.
548 Uchida, Y. Seto, J. R. Goldenring, K. Kakimi, M. Tatematsu, and T. Tsukamoto, Established
549 gastric cancer cell lines transplantable into C57BL/6 mice show fibroblast growth factor receptor
550 4 promotion of tumor growth. **Cancer Science** 109(5), 1480–1492 (2018).

K. Nagaoka, H. Nakanishi, H. Tanaka, J. Anindita, T. Kawamura, T. Tanaka, T. Yamashita, A. Kuroda, S. Nomura, H. Akita, K. Itaka, T. Kodama, and K. Kakimi, Neoantigen mRNA vaccines induce progenitor-exhausted T cells that support anti-PD-1 therapy in gastric cancer with peritoneal metastasis. **Gastric Cancer** 28(5), 825–836 (2025).

E. Darrouzet, S. Lindenthal, D. Marcellin, J.-L. Pellequer, and T. Pourcher, The sodium/iodide symporter: state of the art of its molecular characterization. **Biochimica et Biophysica Acta** 1838(1 Pt B), 244–253 (2014).

T. Watabe, Y. Liu, K. Kaneda-Nakashima, T. Sato, Y. Shirakami, K. Ooe, A. Toyoshima, E. Shimosegawa, Y. Wang, H. Haba, T. Nakano, A. Shinohara, and J. Hatazawa, Comparison of the therapeutic effects of [211At]NaAt and [131I]NaI in an NIS-expressing thyroid cancer mouse model. **International Journal of Molecular Sciences 23**(16), 9434 (2022).

S. Yamamoto, M. Yoshino, K. Kamada, R. Yajima, A. Yoshikawa, K. Nakanishi, and J. Kataoka, Development of an ultrahigh-resolution real-time alpha-particle imaging system for observing the trajectories of alpha particles in a scintillator. **Scientific Reports** 13(1), 4955 (2023).

M. Yoshino, A. Sugiyama, T. Tatsumi, S. Nomura, S. Shimazoe, S. Yamamoto, A. Taguchi, T. Tanaka, M. Kobayashi, and Y. Wada, Observation of At-211 accumulated cells using a real-time alpha-particle imaging system. **RIKEN Accelerator Progress Report**, accepted (2025).

L. Jiang, Y.-Q. Zhu, R. Du, Y.-X. Gu, L. Xia, F. Qin, and H. H. Ritchie, The expression and role of stromal cell–derived factor-1α–CXCR4 axis in human dental pulp. **Journal of Endodontics** 34(8), 939–944 (2008).

S. Yamaguchi, R. Shibata, N. Yamamoto, M. Nishikawa, H. Hibi, T. Tanigawa, M. Ueda, T. Murohara, and A. Yamamoto, Dental pulp–derived stem cell conditioned medium reduces cardiac injury following ischemia–reperfusion. **Scientific Reports** 5, 16295 (2015).

M. Li, X. Sun, L. Ma, L. Jin, W. Zhang, M. Xiao, and Q. Yu, SDF-1/CXCR4 axis induces human dental pulp stem cell migration through FAK/PI3K/Akt and GSK3β/β-catenin pathways. **Scientific Reports** 7, 40161 (2017).

V. C. M. Neves, V. Yianni, and P. T. Sharpe, Macrophage modulation of dental pulp stem cell

activity during tertiary dentinogenesis. **Scientific Reports** 10(1), 20216 (2020).

C. Kornsuthisopon, A. Chansaenroj, J. Manokawinchoke, K. A. Tompkins, N. Pirarat, and T. Osathanon, Non-canonical Wnt signaling participates in Jagged1-induced osteo/odontogenic differentiation in human dental pulp stem cells. **Scientific Reports** 12(1), 7583 (2022).

M. Irfan and S. Chung, C5L2 modulates BDNF production in human dental pulp stem cells via the p38α pathway. **Scientific Reports** 13(1), 74 (2023).

S. Suda, C. Nito, M. Ihara, Y. Iguchi, T. Urabe, Y. Matsumaru, N. Sakai, and K. Kimura; J-REPAIR Trial Group, Randomised placebo-controlled multicentre trial to evaluate the efficacy and safety of JTR-161, allogeneic human dental pulp stem cells, in patients with acute ischaemic stroke (J-REPAIR). **BMJ Open 12**(5), e054269 (2022).

X. Yin, N. Sato, A. Nambu, Y. Shigekawa, and H. Haba, Progress of 211At production at the RIKEN AVF cyclotron. **RIKEN Accelerator Progress Report** 56, 151 (2023).

X. Yin, N. Sato, A. Nambu, Y. Kanayama, Y. Shigekawa, and H. Haba, Modification of 211At

production apparatus to increase its production efficiency. **RIKEN Accelerator Progress Report** 57, 149 (2024).

610 **FIGURE LEGENDS**

611 **Figure 1. Isolation and characterization of dental pulp–derived stem cells (DPCs).**

612 (a) The dental pulp is a soft connective tissue located within the interior of the tooth.

613 (b) After extraction of the dental pulp tissue, the connective components were enzymatically

614 digested, mechanically minced with a sharp blade, and cultured in growth medium supplemented

615 with differentiation inhibitors. Proliferating cells were isolated and purified as dental pulp–

616 derived stem cells (DPCs).

617 (c) Colony-forming assay of DPCs. HeLa cells were used as a control. Cells were stained with a

618 fluorescent dye and cultured for 0 or 7 days. Fluorescence intensity was quantified as relative

619 fluorescence units (RFU; n = 3). Representative microscopic images of colonies are shown. Scale

620 bar, 10 μm.

621

622 **Figure 2. Confirmation of DPC accumulation in peritoneal tumor tissue.**

623 (a–d) Macroscopic and fluorescence imaging analyses of a gastric cancer peritoneal dissemination

624 model after intraperitoneal administration of DiR-labeled dental pulp–derived stem cells (DPCs).

625 Panels (a) and (b) show macroscopic views of the peritoneal serosa, where blue lines outline the

626 regions of peritoneal tumor nodules. Corresponding in vivo imaging system (IVIS) fluorescence

627 images (c and d) demonstrate colocalization of fluorescence signals with the tumor lesions

628 identified in (a) and (b).

629 (e–g) Histological observation of peritoneal tumor tissue 1.5 weeks after intraperitoneal

630 administration of DPCs. Nuclei were counterstained with hematoxylin and eosin stain, and DPCs

631 were detected by immunostaining using an anti-human Lamin B1 antibody followed by an HRP-

632 conjugated secondary antibody. Panel (e) shows a low-magnification image, and (f) shows a high-

633 magnification view of the region. Arrows indicate DPCs accumulated within peritoneal tumor

634 lesions. Panel (g) shows tissue from a normal mouse injected with DPCs as a control.

635 (h) Migration assay evaluating DPC chemotaxis toward YTN16 gastric cancer cells. The lower

636 chamber contained 5×10^4 to 2×10^5 YTN16 cells, and 1×10^5 DiR-labeled DPCs were seeded

637 in the upper chamber. After 48 hours, fluorescence intensity of migrated cells was quantified.

638 DPC migration increased in proportion to the number of YTN16 cells in the lower chamber ($n =$

639 10; $p < 0.001$).

640

641 **Figure 3. Functional transduction of the sodium/iodide symporter (NIS) into dental pulp–**

642 **derived stem cells (DPCs).**

643 (a) Gene expression levels of parental DPCs and sodium/iodide symporter (NIS)–transduced

644 DPCs (NIS-DPCs) quantified from RNA-seq data and presented as transcripts per million (TPM)

645 values. Among iodide symporter genes, SLC5A5 was transduced and expressed in NIS-DPC.

646 GAPDH and beta-actin (ACTB) were controls.

647 (b) Comparison of iodide uptake between DPCs and NIS-DPCs. Data for NIS-DPCs were

648 obtained from three independent donors.

649 (c) Correlation analysis between NIS-positive cell fraction and iodide uptake levels in NIS-DPCs.

650 (d) In vivo localization of NIS-DPCs within tumor tissue, showing accumulation comparable to

651 that of unmodified DPCs.

652 (e) Migration assay using Transwell chambers with YTN16 gastric cancer cells placed in the lower

653 compartment. NIS-DPCs exhibited cell number–dependent migration similar to DPCs ($n = 10$; p

654 < 0.01).

655

656 **Figure 4. Preparation and functional characterization of sodium astatide-211 (Na[At-211])**

657 **and its uptake by NIS-DPCs.**

658 (a) Reaction protocol for converting purified free astatine-211 (At-211), produced at an

659 accelerator facility, into a homogeneous sodium astatide form (Na[At-211]). The free isotope can

660 exist in multiple chemical species, and sodium conjugation was performed to stabilize its form.

661 (b) Thin-layer chromatography (TLC) analysis of At-211 before and after sodium conjugation.

662 Left: TLC profile of free At-211 (~100 kBq). Right: TLC profile of Na[At-211] (~280 kBq).

663 Arrows indicate the Na[At-211] peak position.

664 (c) Cellular uptake of Na[At-211] by dental pulp–derived stem cells (DPCs) and NIS-expressing

665 DPCs (NIS-DPCs). DPCs or NIS-DPCs (5×10^4 cells per well) were seeded in 24-well plates and

666 incubated with 10 kBq Na[At-211]. At 5, 10, and 60 min, cells were collected, fractionated, and

667 measured for protein concentration and radioactivity. Radioactivity normalized to protein content

668 was calculated. NIS-DPCs exhibited approximately tenfold higher At-211 uptake than parental

669 DPCs (n = 3; black bars, DPCs; gray bars, NIS-DPCs).

670

671 **Figure 5. Detection of α-particle emission from NIS-transduced dental pulp–derived stem**

672 **cells (NIS-DPCs).**

673 (a) Schematic diagram of the α-particle detection system. α-particles emitted from cells (left) are

674 first converted into photons by a GAGG:Ce scintillator. The photons are then amplified and

675 reflected within the detector and captured by a cooled CMOS sensor positioned at the top.

676 (b) Overview of the α-particle detection device.

677 (c–d) NIS-DPCs (1×10^4 cells per well) were seeded in 8-well chamber slides and incubated for

678 30 min with 500 kBq of sodium astatide–211 (Na[At-211]). Cells were then fixed with formalin

679 and imaged. Arrowheads indicate the localization of individual cells.

680 (f–h) DPCs (1×10^4 cells per well) were similarly treated with 500 kBq Na[At-211], incubated

681 for 30 min, fixed with formalin, and imaged. Arrowheads indicate cell localization.

682 (c and f) Optical microscopic images of cells. (d and g) Corresponding α-camera signal images.

683 (e and h) Merged images combining optical and α-particle signals. Scale bar, 100 μm.

684

685 **Figure 6. Therapeutic efficacy of NIS-DPCs combined with At-211 in a murine gastric**

686 **cancer peritoneal dissemination model.**

687 C57BL/6 mice were inoculated intraperitoneally with 1×10^7 YTN16 gastric cancer cells to

688 establish a peritoneal dissemination model. One week later, 0.5×10^6 NIS-DPCs were

689 intraperitoneally administered every other day for three doses. Three days after the final cell

690 transplantation, 0.6 MBq of sodium astatide-211 (Na[At-211]) was injected intraperitoneally, and

691 mice were sacrificed 1.5 weeks later for macroscopic observation.

692 (a) Untreated control group.

693 (b–d) Mice receiving one, two, or three intraperitoneal administrations of NIS-DPCs followed by

694 Na[At-211], respectively. Peritoneal tumor burden decreased in proportion to the number of NIS-

695 DPC treatments.

696 (e) Macroscopic scoring of peritoneal dissemination was performed on a 0–4 scale.

697 (f) Quantitative comparison of macroscopic scores among the untreated group, Na[At-211]-only

698 group, and the group receiving three NIS-DPC administrations plus Na[At-211]. Statistical

699 analysis was performed using Tukey's test ($n = 10$; $p < 0.01$, $^*p < 0.001$).

700 (g) Kaplan–Meier survival analysis after one month following Na[At-211] administration. Mice

701 treated with three doses of NIS-DPCs plus Na[At-211] (#3) showed a significant survival

702 advantage compared with the untreated group (#1) and the Na[At-211]-only group (#2). Control

703 groups without YTN16 cell implantation included Na[At-211]-only (#5) and NIS-DPC × 3 +

704 Na[At-211] (#6) treatments (n = Y; p <○○, *p < ○○).

705

706 **Figure 7. Graphical Summary. Stepwise overview of the NIS-DPC cancer-targeting concept.**

707 The schematic illustrates the translational workflow of sodium/iodide symporter (NIS)–

708 expressing dental pulp–derived stem cells (NIS-DPCs) as a targeted theranostic platform for

709 cancer therapy.

710 Step 1 (engineering). Dental pulp–derived stem cells were genetically modified to express the

711 sodium/iodide symporter (NIS), which mediates the cellular uptake of both iodide and astatine.

712 The lower panel depicts this dual transport function of NIS, highlighting its ability to internalize

713 iodide and the α-emitting radionuclide At-211.

714 Step 2 (targeting and accumulation). Following administration, NIS-DPCs preferentially

715 accumulated in cancer cells, enabling the selective delivery of At-211 to tumor sites.

716 Step 3 (localized therapy/outcome). Localized α radiation at the tumor site induced targeted

717 cytotoxicity, demonstrating the translational potential of NIS-DPC–mediated therapy for precise

718 cancer treatment.

719

TITLE

Novel therapy for gastric cancer peritoneal dissemination using genetically modified dental pulp cells and astatine-211

AUTHORS

Koumei Kuge[1,2], Wan-Ying Du[1], Hiroki Masuda[1,2], Tomohiko Yasuda[1,2], Toshifumi Tatsumi[3], Xiaojie Yin[4], Masao Yoshino[5], Akira Sugiyama[6], Ryohei Numata[7], Wataru Yokoyama[7], Hidenori Shibahara[7], Tomoko Tanaka[3], Mika Kobayashi[3], Akashi Taguchi[3], Takahide Kohro[8], Naoko Takubo[3], Masahiro Nakamura[3], Jaewoong Jang[3], Yoshitaka Kumakura[3,9], Hiroshi Yoshida[2], Akira Yoshikawa[5,10], Hiromitsu Haba[4], Youichiro Wada[3]*, Kiwamu Imagawa[7]**, and Sachiyo Nomura[1,3,6]***

CORRESPONDENCE

*Co-corresponding author. Email: wada-y@ric.u-tokyo.ac.jp

** Co-corresponding author. Email: imagawa-k@jp.jcrpharm.com

*** Co-corresponding author. Email: sachiyo.nomura1012@gmail.com

AFFILIATIONS

19 [1] Department of Gastrointestinal Surgery, Graduate School of Medicine, The University of Tokyo

20 [2]Department of Surgery, Graduate School of Medicine, Nippon University

21 [3]Isotope Science Center, The University of Tokyo

22 [4]Nishina Center for Accelerator-Based Science, RIKEN

23 [5]Institute for Materials Research, Tohoku University

24 [6]School of Pharmacy and Pharmaceutical Sciences, Hoshi University Clinical Pharmaceutical

25 Sciences

26 [7]Regenerative Medicine Unit, Drug Discovery Research Institute, Research Division, JCR

27 Pharmaceuticals Co., Ltd.

28 [8]Department of Cerebrovascular Medicine, Jichi Medical School

29 [9]Department of Diagnostic Radiology and Nuclear Medicine, Saitama Medical Center, Saitama

30 Medical University

31 [10]New Industry Creation Hatchery Center, Tohoku University

32

33 **SUMMARY**

34 Peritoneal dissemination of gastric cancer represents a terminal stage with limited therapeutic

35 options and a five-year survival rate below 10%. To develop a more effective treatment, we

36 established a novel α-particle–based approach using genetically engineered human dental pulp

stem cells (DPCs) expressing the sodium/iodide symporter (NIS) to deliver astatine-211 (At-211) directly to tumor sites. DPCs, isolated and expanded under differentiation-suppressive conditions, showed strong tumor-homing ability when injected intraperitoneally into a mouse model of gastric cancer dissemination. Fluorescent imaging and histological analysis confirmed selective accumulation of DPCs within tumor lesions through CXCR4/SDF-1–mediated chemotaxis. Introduction of the NIS gene markedly increased SLC5A5 expression and enabled efficient uptake of At-211. High-resolution α-particle imaging visualized α-ray emission specifically from NIS-DPCs, confirming intracellular retention of the radionuclide. *In vivo*, sequential administration of NIS-DPCs followed by At-211-Na led to pronounced regression of peritoneal tumors and significant survival extension compared with controls. The therapeutic mechanism involves three coordinated steps: tumor-directed migration of NIS-DPCs, At-211 uptake via NIS transporters, and localized α-particle–mediated cytotoxicity. This study introduces a novel concept of cell-based α-radiotherapy integrating regenerative and nuclear medicine. Given the established clinical safety of DPCs in humans (J-REPAIR, jRCT1080224505), this NIS-DPC platform offers a promising strategy for precise, short-range irradiation of disseminated gastric cancer and potentially other intractable malignancies.

INTRODUCTION

55 Peritoneal dissemination is a common terminal manifestation of gastric cancer and is
56 classified as stage IV disease, with a 5-year survival rate of less than 10%. Current therapeutic
57 options are largely palliative, highlighting an urgent need for new treatment strategies with
58 curative potential.

59 We previously established a murine gastric cancer peritoneal dissemination cell line
60 (YTN16) and demonstrated proof-of-concept efficacy of targeted α-particle therapy using
61 astatine-211 (At-211), a high–linear energy transfer radionuclide with a 7.2-hour half-life. An
62 anti–fibroblast growth factor receptor 4 (FGFR4) antibody—selected for its high expression on
63 YTN16 cells—was conjugated to At-211 via a halogen–tin exchange reaction. In vivo
64 biodistribution studies in a syngeneic C57BL/6J peritoneal dissemination model showed that
65 intraperitoneal administration achieved peak peritoneal radioactivity at 4.5 hours, resulting in
66 marked tumor regression and significant survival extension compared with untreated controls.

67 However, the therapeutic window is constrained by the mismatch between the time
68 required for antigen–antibody binding (~24 hours) and the physical half-life of At-211. To
69 improve delivery kinetics, we sought a vehicle capable of rapidly homing to the tumor
70 microenvironment. Tumors actively recruit stromal fibroblasts to form cancer-associated
71 fibroblasts (CAFs), and mesenchymal cells (MSCs) share similar tumor-tropic properties. We

72 therefore investigated dental pulp cells (DPCs) developed by JCR Pharmaceuticals, which have
73 an established manufacturing process and demonstrated safety in a phase 1/2 clinical trial for
74 acute ischemic stroke (Ref. jRCT1080224505).

75 Here, we evaluate DPCs as a biologic vector for targeted α-particle therapy in gastric
76 cancer peritoneal dissemination. We hypothesize that leveraging the tumor-homing ability of
77 DPCs can facilitate At-211 delivery to the tumor niche, overcoming the limitations of
78 radioimmunotherapy and enabling improved therapeutic efficacy and survival outcomes.

79

80

81

82 **RESULTS**

83 **Preparation and characteristics of DPCs**

84 Dental pulp cells are located in the dental pulp, the soft connective tissue found in the
85 center of teeth (Figure 1a). They play key roles in tooth vitality by producing dentin, supporting
86 sensory functions, and participating in immune defense and tissue repair (Ref. Nito).

87 Dental pulp extraction is followed by mild enzymatic digestion to loosen the
88 extracellular matrix, then mechanical mincing to produce small tissue pieces. These explants are
89 placed in culture, allowing maintenance and expansion of dental pulp cells (DPCs) (Ref.
90 Gronthos) (Figure 1b).

91 DPCs could be expanded using culture medium, but no proliferation was observable in
92 soft agar, suggesting no tumorigenicity after injecting *in vivo* (Figure 1c).

93

94 **Confirmation of DPC accumulation in peritoneal tumor tissue**

95 To investigate that DPCs harbor the ability of tumor accumulation, we applied them into
96 the peritoneal cavity of gastric cancer dissemination model, which was established previously by
97 us (Ref.Yamamoto). Firstly, 5 x10^5 cells of DPCs were prepared as described in materials and
98 methods. Then they were labeled with fluorescence dye (DiR) for living cells. After 24 hours,
99 injected mouse models were euthanized, and peritoneal surface was opened to apply florescence

100 detection camera. Localization of injected DPCs was visualized using in vivo imaging system
101 (IVIS Lumina III), and compared with distribution of disseminated visible lesions. As shown in
102 Figure 2, lesion occupied area was surrounded by blue line (right in Figure 2a, left in 2b).
103 Fluorescent images obtained by fluorescent camera was shown in Figure 2c (left) and 2d (right).
104 Significant colocalization was observable in both sides, suggesting accumulation of DPCs to
105 gastric cancer cells.

106 To further evaluate the specificity of tumor-directed accumulation, 1.0×10^6 DPCs were
107 injected intraperitoneally into a gastric cancer mouse model. Two days after the last injection of
108 DPCs, mice were sacrificed, and peritoneal tissues were fixed and subjected to
109 immunohistochemical staining using an anti-human Lamin B1 antibody. Brown staining,
110 indicative of DPC localization, was observed in tissues surrounding established tumor lesions
111 (Figure 2e, f), whereas no staining was detected in tissues lacking tumor cell engraftment (Figure
112 2g). These findings strongly suggest that intraperitoneally administered DPCs migrate to and
113 accumulate within peritoneal dissemination sites.

114 To validate the migratory ability of the DPCs towards the YTN16 cell line, a migration
115 assay was performed using a Transwell chamber. After $1x10^5$ DPCs were placed in the upper
116 chamber, a series of different numbers of YTN16 cells were placed in the lower chamber. The
117 migrated cells on the other side of the micropore membrane were stained with a Calcein solution,

118 and the absorbance was measured. Figure 2h shows that the presence of YTN16 cells induces
119 DPC migration in a cell number-dependent manner and proves the migration capability of DPCs
120 to YTN16 cells.
121
122 **Functional transduction of NIS to DPC**
123 The sodium-iodide symporter (NIS) is a transmembrane glycoprotein with 13
124 transmembrane domains that transports radioactive isotopes, such as I-131, I-123, I-125, I-124,
125 Tc-99m, Re-188, and At-211, into cells (Ref. Darrouzet). Therefore, we introduced the NIS gene
126 (SLC5A5) into DPC cells using lentivirus (Figure 3a). While there was no change in the
127 expression levels of other NIS-encoding genes, such as SLC26A4 and SLC26A7, the expression
128 level of SLC5A5 in NIS-DPC increased more than 100-fold.
129 Next, we verified the expression level of NIS molecules on the cell surface and
130 evaluated the correlation between uptake capacity and positive rate using iodine as a surrogate
131 molecule in vitro. The results are shown in Figure 3b and 3c. We confirmed that iodine uptake
132 increased in a NIS-positive rate-dependent manner and observed a trend where higher NIS-
133 positive rates correlated with higher iodine uptake (Figure 3c). When iodine uptake was
134 confirmed in three lots of NIS-DPC cells, more iodine uptake was observed compared to DPC

135 cells without gene introduction. This confirmed that the introduced NIS gene was expressed on

136 the cell surface and that its function was maintained (Figure 3b).

137 To validate that NIS-DPCs could migrate to dissemination lesions, NIS-DPCs were

138 injected into the peritoneal cavity, as was done with DPCs. Two days after injection, the peritoneal

139 tissues were subjected to immunohistochemical staining using an anti-human lamin B1 antibody.

140 As shown in Figure 2e and 2f, brown staining indicative of NIS-DPC localization was observed

141 in tissues surrounding established tumor lesions (Figures 3d and 3e), whereas no staining was

142 detected in tissues lacking tumor cell engraftment (Figure 3f). These findings strongly suggest

143 that the NIS-DPCs administered intraperitoneally were able to accumulate within peritoneal

144 dissemination lesions.

145

146 **Uptake of At-211 by NIS-DPC**

147 Recently, it has been reported that, due to its various chemical forms, purified At-211

148 undergoes nonspecific binding in vivo, and that this can be controlled by converting it to sodium

149 astatine-211 (Ref. Watabe 2022). Therefore, prior to in vivo administration, we prepared sodium

150 astatine-211 using the method shown in Figure 4a. We confirmed that the purified At -211 had a

151 uniform chemical form using thin layer chromatography (TLC) (Figure 4b).

Furthermore, we confirmed the amount of At-211 that was taken up by the cells. The results are shown in Figure 4c. As with the results of the confirmation of uptake capacity using a surrogate molecule, NIS-DPC cells with the introduced NIS gene took up more At-211 than DPC cells without the introduced gene. Additionally, the highest uptake was observed at 5 minutes when comparing changes in uptake amount over time at 5, 10, and 60 minutes after At-211 addition. These results suggest that At-211 is rapidly taken up by DPC cells via NIS. Therefore, pre-accumulating NIS-DPC cells around the peritoneal dissemination site and then administering At-211 allows the drug to be taken up by cells quickly enough to be effective within its half-life.

Novel contact scintillator imaging of alpha-ray trajectories from alpha emitters

Because the NIS-DPC cell fraction is radioactive, the uptake of At-211 was suggested. However, to verify that the alpha rays emitted from At-211 originate from the NIS-DPC cells, a camera that can visualize alpha rays on a 1 μm scale was used. Figure 5a shows the alpha camera system configuration (Ref. Yamamoto 2023) (Ref. Yoshino 2025). It comprises three principal components: (i) a 100-μm-thick GAGG thin-film scintillator screen; (ii) an infinity-corrected magnification optical train consisting of an objective, an imaging lens; and (iii) a CMOS imaging sensor, specifically the ORCA-Quest 2 qCMOS (C15550-22UP) from

170 Hamamatsu Photonics. Alpha particles emitted from within the cells are converted into photons
171 by a GAGG scintillator, magnified by a 20x objective, and detected by a CMOS sensor. Figure
172 5b shows an overview of the system. Eighteen thousand NIS-DPC and DPC cells were cultured
173 in an eight-well chamber slide. Then, 500 kBq of At-211 was added to the culture medium per
174 well, followed by a 30-minute incubation period. The cells were then fixed with formalin, and
175 observation with an alpha camera was conducted for ten minutes. Figure 5c shows an overview
176 of the NIS-DPC cells and Figure 5f shows an overview of the DPC cells. Both exhibit similar
177 morphology and distribution. However, as Figures 5d and 5g show, the alpha particle range was
178 detected only in the NIS-DPC cells. The merged image in Figure 5h confirms localization in the
179 NIS-DPC cells. These results indicate that At-211 was efficiently taken up by NIS-DPC cells
180 and that α-rays were emitted from these cells.
181
182 **At-211 and NIS-DPC cell administration showed antitumor effects**
183 Then, we preliminarily assessed the antitumor and survival prolongation effects of At-
184 211 and NIS-DPC administration in a mouse peritoneal dissemination model. Three weeks after
185 tumor cell transplantation, 0.5×10^6 NIS-DPC cells were administered intraperitoneally.
186 Twenty-four hours later, 0.6 MBq of astatine-211 was administered per animal. At one and a
187 half weeks post-transplantation, examination of the peritoneum revealed tumor cells in the

188 peritoneal dissemination group (Figure 6a), as well as in the NIS-DPC administration group
189 (Figure 6b) and the astatine-211 administration group (Figure 6c). However, the disappearance
190 of peritoneal seeding was observed in the group that received both NIS-DPC and astatine-211
191 (Figure 6d, asterisks).

192 To evaluate the effect of NIS-DPC&At-211 treatment, we scored the antitumor effects
193 visually on a 5-point scale (0–4) based on the extent of cancer cells adhering to the peritoneal
194 tissue at the time of death or at the end of the observation period (Figure 6e). We then evaluated
195 the results using the Tukey test.

196 The results of the antitumor effect evaluation are shown in a box-and-whisker plot
197 (Figure 6f). Compared to the untreated group (No Treatment) and the At-211 monotherapy
198 group (At-211), a significant reduction in score (i.e., reduction in disseminated tissue) was
199 observed in the At-211+NIS-DPC group (At-211+NIS-DPC). It was therefore suggested that the
200 administered NIS-DPC accumulated around implanted cancer cells in the peritoneum.
201 Subsequently, the cancer tissue was reduced by the cytolytic effect of α-rays after the uptake of
202 the administered At-211.

203 Using the same evaluation scale, we performed a series of experiments to optimize the
204 radioactivity of At-211 (Figure S6a), dose of NIS-DPC (Figure S6b), and repetition of NIS-DPC
205 injection (Figure S6c). Based on the macroscopic evaluation of the extent of peritoneal

206 dissemination, 0.6MBq of At-211/body, $5x10^5$/body of NIS-DPC, three-time administration of

207 NIS-DPC, provided significantly higher score.

208 Using this optimized regimen, survival rates were evaluated using Kaplan-Meier

209 curves and Logrank tests. The survival rates of individual mice in each group after At-211

210 administration were evaluated. The results are shown in Figure 6g. Compared to the untreated

211 group and the At-211 treated group, a significant prolongation of survival was observed in the

212 At-211 + NIS-DPC group. Based on these results, the extension of the survival rate is

213 considered to be due to the damage and reduction of the implanted tumors by At-211 and NIS-

214 DPC in the mouse peritoneal dissemination model.

215

216

DISCUSSION

Brief summary

In this study, we created NIS-DPC cells by forcing the expression of the NIS gene, which encodes an iodine transporter, in DPC cells that accumulate in the peritoneal cavity. Forty-eight hours after administering these cells, we introduced astatine-211 into the peritoneal cavity, demonstrating that the NIS-DPC cells accumulated around the tumor cells were rapidly taken up, resulting in tumor cell death. This three-step treatment method is illustrated in Figure 7: addition of NIS-DPC cells, addition of At-211, and α-ray irradiation. The first process involves the accumulation of NIS-DPC cells in tumors. The second process involves the uptake of astatine-211 by NIS-DPC cells. The third process involves tumor-killing effects.

Accumulation of DPC/NIS-DPC to cancer cells

It is known that cancer cells accumulate large numbers of cancer-associated fibroblasts (CAFs) in their vicinity. However, mesenchymal stem cells (MSCs) exhibit similar dynamics to CAFs. MSCs migrate in response to chemokines, such as SDF-1, produced by cancer cells. They recognize these chemokines via CXCR4. However, due to protein cross-reactivity between humans and mice, human MSCs can migrate toward mouse tumors as well. Additionally, MSCs have low immunogenicity and can be administered allogeneically. Since 2008, when it was

235 reported that DPC cells (a type of MSC) express CXCR4 and migrate in response to SDF-1 (Ref.
236 Jiang 2008), it has frequently been reported that DPC cells accumulate in inflammatory or
237 ischemic sites, particularly in oral and maxillofacial surgery (Ref. Yamaguchi et al., Sci. Rep.
238 2015) (Ref. Li et al., Sci. Rep. 2017)(Ref. Neves et al., Sci. Rep. 2020)(Ref. Kornsuthisopon et
239 al., Sci. Rep. 2022) (Ref. Irfan et al., Sci. Rep. 2023). DPCs produced by JCR Pharmaceuticals,
240 which have been administered to humans and proven safe (Ref. Suda 2022), were examined for
241 their ability to migrate and accumulate around tumor tissues in a mouse peritoneal dissemination
242 model.

243 As mentioned above, the first process of this therapy is accumulation of DPC cells to
244 cancer cells. To prove this, multimodal experiments were performed. Macroscopically, as shown
245 in Figures 2a to 2d, the localization of fluorescently labeled DPC cells coincided with the
246 localization of gastric cancer peritoneal dissemination lesions. Microscopically, as shown in
247 Figures 2e to 2g, DPC cells were observed within gastric cancer lesions via immunohistochemical
248 staining. These findings indicate that DPC cells accumulate in tumor cells.

249 In vitro, DPC cells were observed migrating toward gastric cancer cells (Figure 2h).
250 However, the molecular mechanism underlying this migration is suggested to involve the
251 induction of EGR1 in DPC cells by soluble factors released from cancer cells. Further clarification
252 of the migration mechanism is needed in further study.

253

254 **Functional uptake of At-211 by NIS-DPC**

255 The second step of this treatment method involves the uptake of At-211 by DPC cells.
256 Several experiments were conducted to determine if the introduced iodine transporter functions
257 in DPC cells. First, non-radioactive iodine and a non-radioactive ligand were added to DPC cells
258 expressing NIS, and the uptake efficiency was examined. As Figures 3b and 3c show, DPC cells
259 expressing NIS exhibited approximately 50-fold higher iodine uptake. The amount of uptake
260 increased in a NIS expression-dependent manner, demonstrating that NIS functionally takes up
261 the ligand. Furthermore, Figure 4c shows efficient uptake of At-211 by NIS-DPC starting five
262 minutes after At-211 addition. Using the newly developed α camera, we confirmed that the uptake
263 of At-211 and cell localization were consistent. This indicates that NIS-DPC cells take At-211
264 into the cell and emit α rays. In the future, it is expected that the lethal effect of α rays on tumor
265 cells will be directly visualized by co-culturing NIS-DPC cells with tumor cells and observing
266 them using the α camera.

267

268 **Tumoricidal effect of NIS-DPC&At-211**

269 As shown in Figure 6, this study demonstrated that administering At-211 after NIS-DPC
270 administration reduced peritoneal dissemination lesions and prolonged survival. This confirms

271 the tumor-killing effect, which is the third process in this treatment. In the evaluation of anticancer
272 drug efficacy in humans, the primary endpoint is survival rate extension. Therefore, when
273 evaluating the efficacy of cancer treatments using model animals, improvement in survival rate is
274 equally important as it is in humans. Furthermore, the proposed mechanism of action was strongly
275 implicated. However, it has been reported that immune function induced by neoantigens released
276 from tumor cells damaged by radiation exposure contributes to the efficacy of nuclear medicine
277 therapy (Ref. Nagaoka). Elucidating the detailed mechanism in the future may expand the
278 application of combined therapy with NIS-DPC cells and astatine-211.
279
280 **Requirement for practical application**
281 To commercialize this treatment method in the future, data on its efficacy must be
282 accumulated. Additionally, data on the safety and pharmacokinetics of the reagents used in this
283 study will be necessary. Since DPC cells have been administered to humans before and their safety
284 has been demonstrated (Ref. Suda 2022), data on the safety of NIS-DPC is necessary. In particular,
285 since lentiviruses are used to introduce the NIS gene, it is necessary to clarify whether they are
286 excreted from the administered animals. Furthermore, since astatine-211 is administered in the
287 form of sodium astatine into the abdominal cavity, pharmacokinetic data must be obtained in
288 medium-sized animals prior to human administration. Human clinical studies will be conducted

289 based on these data.

290 DPC cells can be administered allogenically. Since their procurement is minimally
291 invasive, the cells can be stored frozen, which makes it feasible to establish a supply system.
292 Additionally, meeting clinical demand for At-211 is possible through the future widespread
293 adoption of mass production technology and the development of dedicated accelerators.

294

295 **Perspective**

296 Here, we reported a new treatment method combining nuclear and regenerative
297 medicine products. Since the safety of DPC cells has already been proven in humans, a first-in-
298 human trial should be conducted after the safety of NIS-DPC and At-211 is evaluated.

299

300

301

302

303

304 **MATERIALS AND METHODS**

305 **Preparation of Dental Pulp Cells (DPCs)**

306 Human dental pulp cells (DPCs) were isolated from extracted teeth under sterile
307 conditions, as previously described with minor modifications. Briefly, extracted teeth were first
308 disinfected by immersion in 1% formalin solution followed by washing with sterile physiological
309 saline to remove debris and surface contaminants.

310 The tooth structure was mechanically fractured using a dental rongeur, and the pulp
311 tissue was carefully extracted from the pulp chamber. The obtained pulp tissue was minced into
312 small fragments using sterile surgical scissors and transferred into a tube containing Liberase
313 digestion solution (Roche Diagnostics, Basel, Switzerland). The tissue suspension was incubated
314 at 37°C for enzymatic digestion with gentle agitation until the connective matrix was adequately
315 loosened.

316 After digestion, the suspension was mixed with Dulbecco's Modified Eagle Medium
317 (DMEM) supplemented with 10% fetal bovine serum (FBS) and 1% penicillin/streptomycin (P/S)
318 to terminate the enzymatic reaction. The mixture was centrifuged at 300 × g for 5 min, and the
319 supernatant was discarded. The resulting pellet was resuspended in fresh DMEM containing 10%
320 FBS and 1% P/S and seeded onto tissue culture plates.

321 Cells were incubated at 37°C in a humidified 5% CO_2 atmosphere and expanded until

322 passage 5 (P5). From passage 1 (P1) onward, cultures were maintained in DMEM supplemented
323 with 10% FBS but without antibiotics, to avoid potential effects of antimicrobial agents on cell
324 proliferation or differentiation. All procedures were conducted under aseptic conditions using
325 biosafety level 2 (BSL-2) practices.
326
327 **Soft Agar Colony Formation Assay**
328 To evaluate anchorage-independent growth and confirm the non-transformed
329 characteristics of the cells, a soft agar colony formation assay was performed using the
330 CytoSelect™ 96-Well Cell Transformation Assay Kit (Cell Biolabs, Inc., San Diego, CA, USA),
331 according to the manufacturer's protocol.
332 HeLa, DPC, and NIS-DPC cells were cultured under standard conditions until reaching
333 logarithmic growth phase. Cells were then harvested and resuspended in assay medium at the
334 following densities: 8×10^3 cells/well for HeLa, and 8×10^4 cells/well for DPC and NIS-DPC.
335 Cell suspensions were seeded in duplicate 96-well soft agar plates (Plate ① and Plate ②) as
336 described in the kit instructions.
337 Plate ① was incubated for 7 days at 37°C in a humidified 5% CO_2 incubator to allow
338 potential colony formation. Plate ② was processed immediately after cell seeding for background
339 measurement following the manufacturer's procedures: agar dissolution, cell lysis, and nuclear

340 staining. The absorbance of each well was measured using a microplate reader to determine
341 baseline optical density (OD).
342 After the 7-day incubation period, Plate ① was subjected to the same lysis and staining
343 procedures, and absorbance was measured again. Colony formation was quantified by comparing
344 OD values between the 0-day (Plate ②) and 7-day (Plate ①) samples. As expected, a significant
345 increase in OD was observed only in the HeLa group, while DPC and NIS-DPC cells showed no
346 increase, confirming their non-transformed phenotype.
347
348 **Preparation of mouse model and application of NIS-DPC followed by Na[At-211]**
349 Six-week-old female C57BL/6J mice were purchased from Jackson Laboratoy Japan
350 and housed in a specific pathogen-free environment at the Animal Experiment Facility in
351 Isotope Science Center, the University of Tokyo. The animal use proposal and experimental
352 protocol were reviewed and approved by the University of Tokyo Animal Committee (ID: Med-
353 P22-084、A2024ISC003). The YTN16 cell line was maintained in Dulbecco's modified
354 Eagle's medium (DMEM, Sigma-Aldrich Merck, Tokyo, Japan) with 10% heat-inactivated fetal
355 bovine serum (FBS, BWT, France), 50 μg/mL streptomycin, 50 U/mL penicillin
356 (ThermoFisher, Tokyo, Japan), and MITO + serum extender (Corning, Corning, NY, USA). A
357 total of 1×10^7 YTN16 cells were suspended in 500 μL of Hanks' Balanced Salt Solution and

358 intraperitoneally injected into mice (Ref. Nagaoka). Starting the following day, 2 μg of

359 thyroxine was administered orally once daily. At 8, 10, and 12 days after YTN16 cell injection,

360 1×10^6 NIS-DPC cells, 1×10^6 DPC cells, or vehicle alone were administered intraperitoneally.

361 On day 14, Na[At-211] (0.6 MBq) dissolved in 0.5 mL of vehicle was injected

362 intraperitoneally. On day 35 after YTN16 cell injection, the peritoneal cavity was examined, or

363 the mice were observed until death or humane sacrifice, followed by examination of the

364 peritoneal cavity.

365

366 **Construction of Lentiviral Vector pLVSIN-EF1α-hNIS-Pur**

367 A self-inactivating (SIN) lentiviral expression vector, pLVSIN-EF1α-hNIS-Pur, was

368 constructed based on the parental plasmid pLVSIN-EF1α-Pur (Takara Bio Inc.). The human

369 sodium/iodide symporter (hNIS) gene (sequence ID No. 2; NCBI accession number

370 NM_000453.3) was inserted into the multiple cloning site of the parental vector.

371 The DNA fragment encoding hNIS was synthesized with a Not I site at the 5′ end and a BamH I

372 site at the 3′ end. Both the hNIS insert and the pLVSIN-EF1α-Pur vector were digested with the

373 respective restriction enzymes Not I and BamH I (New England Biolabs or equivalent) to

374 generate compatible cohesive ends. The digested fragments were ligated using Ligation High

375 Ver. 2 (TOYOBO Co., Ltd.), yielding the recombinant plasmid pLVSIN-EF1α-hNIS-Pur.

376 All recombinant DNA manipulations were carried out under standard molecular cloning

377 conditions in accordance with institutional biosafety regulations.

378

379 **Lentiviral Packaging and Production**

380 Lentiviral particles carrying the pLVSIN-EF1α-hNIS-Pur construct were produced

381 using a self-inactivating lentiviral packaging system. In addition to the expression vector

382 described above, a mixture of packaging plasmids encoding HIV-1–derived structural and

383 regulatory proteins (Gag, Pol, Tat, and Rev) and the vesicular stomatitis virus G glycoprotein

384 (VSV-G) envelope was provided by the Lentiviral High Titer Packaging Mix (Takara Bio Inc.).

385 Viral particles were generated following a modified standard protocol.

386 Poly-L-lysine–coated culture dishes were seeded with cells at a density of

387 approximately 5×10^4 cells/cm² and incubated overnight at 37°C in a humidified 5% CO_2

388 incubator. On the following day, a DNA mixture was prepared by adding 7 μL of Packaging Mix

389 and 11 μL of pLVSIN-EF1α-hNIS-Pur plasmid DNA (0.5 μg/μL) to 1.5 mL of Opti-MEM I

390 Reduced Serum Medium (Gibco).

391 Transfection was performed using either FuGENE HD (Promega) or TransIT-Lenti Transfection

392 Reagent (Takara Bio Inc.), according to the manufacturers' instructions. The transfected cells

393 were incubated at 37°C in 5% CO_2 for approximately 24 hours, after which the culture supernatant

394 was replaced with 10 mL of DMEM (Gibco) and incubation continued for another 24 hours.

395 The culture supernatant containing lentiviral particles was collected and clarified by

396 centrifugation at 500 × g for 10 minutes. The supernatant was then passed through a 0.45 μm filter

397 (Millipore, Cat. No. SLHPR33RB) to remove cellular debris. The filtered viral solution was

398 aliquoted into microtubes and stored at −80°C until use.

399

400 **Generation of hNIS-Expressing Dermal Papilla Cells (hNIS-DPCs)**

401 Dental pulp cells (DPCs) were seeded at a density of 2.0×10^4 cells/cm² and cultured

402 overnight at 37°C in a humidified 5% CO_2 incubator. On the following day, cells were transduced

403 with the hNIS lentiviral vector (hNIS-LV) at a multiplicity of infection (MOI) of 10. To enhance

404 viral transduction efficiency, protamine sulfate (Sigma-Aldrich, Cat. No. P4020) was added to

405 the viral inoculum at a final concentration of 100 μg/mL.

406 The viral supernatant was removed 24 hours after infection and replaced with fresh

407 DMEM (Gibco, Cat. No. 10567-014). Cells were cultured with medium changes every 2–3 days,

408 and cell morphology and confluence were monitored microscopically. When cultures reached

409 approximately 90% confluence, cells were passaged using standard trypsinization procedures.

410 For selection of transduced cells, puromycin was added to the culture medium at a final

411 concentration of 1 μg/mL during the first passage after viral infection. Resistant colonies were

412 expanded under puromycin selection. Thereafter, cells were maintained in standard DMEM
413 without selection antibiotic for one to two additional passages to establish a stable hNIS-DPC line.
414 Established cells were cryopreserved in liquid nitrogen for long-term storage.
415
416 **Cell Culture**
417 NIS-DPC and YTN16 cells were cultured in Dulbecco's modified Eagle's medium
418 (DMEM; Gibco, Cat. No. 10567014) under standard conditions (37°C, 5% CO_2). Cells were
419 maintained for 3 to 4 days before use.
420
421 **Cell Harvesting and Co-culture Setup**
422 Cells were detached using 0.25% trypsin–EDTA (Gibco, Cat. No. 25200056) and
423 resuspended in fresh DMEM. Cell concentrations were adjusted to 1×10^5 cells/mL. For co-
424 culture experiments, cells were seeded into 24-well Transwell plates (Corning, Cat. No. 353504)
425 equipped with cell culture inserts (Corning, Cat. No. 351152). NIS-DPC cells (1×10^5 cells) were
426 seeded in the upper insert, and YTN16 cells (1×10^5 cells) were seeded in the lower chamber. The
427 co-cultures were incubated for 48 hours at 37°C in a humidified incubator with 5% CO_2.
428
429 **Migration assay**

430 After 48 hours of co-culture, the medium was aspirated and replaced with DMEM
431 containing 1% human serum albumin (HSA) prepared from 25% clinical-grade albumin solution
432 (Takeda Pharmaceutical Co., Ltd.). Cells were stained with Calcein (Dojindo, Cat. No. 341-
433 07901) according to the manufacturer's instructions to visualize viable cells. Fluorescence
434 intensity was quantified using a spectrophotometric plate reader, and fluorescent images were
435 captured using a fluorescence microscope under identical exposure conditions for all samples.

436

437 **Cell Labeling with DiR and In Vivo Administration**

438 NIS-DPC cells were suspended in medium at a concentration of 1×10^7 cells/mL. The
439 cell suspension was mixed with an equal volume of 20 μmol/L DiR dye solution (Thermo
440 Fisher Scientific or equivalent), resulting in a final dye concentration of 10 μmol/L. The mixture
441 was incubated for 15 minutes at room temperature in the dark, with gentle tapping every 5
442 minutes to ensure homogeneous labeling. After incubation, the cells were washed three times
443 with injection medium by centrifugation to remove excess dye. The labeled cells were
444 resuspended in injection medium at a final concentration of 1×10^6 cells/mL. Labeled NIS-DPC
445 cells were administered intraperitoneally to peritoneal dissemination model mice. All animal

experiments were conducted in accordance with institutional guidelines and approved by the relevant Animal Care and Use Committee.

In Vivo Fluorescence Imaging

At predetermined time points after injection, mice were sacrificed, and peritoneal tissues were harvested. DiR fluorescence signals were detected using an in vivo imaging system (IVIS Lumina III; PerkinElmer) under the following parameters: excitation filter, 740 nm; emission filter, 790 nm; and exposure time, automatic setting. Fluorescence images were analyzed using the manufacturer's software.

Production of ^{211}At

According to the procedure described in Refs. (Yin 2023, Yin 2024), the radioisotope of At-211 was produced in the nuclear reaction of ^{209}Bi(α,2n)^{211}At using the AVF cyclotron of the RIKEN RI Beam Factory.

Ppreparation of Na[At-211]

462 Dry solid At-211 of multiple chemical species in glass vial was dissolved the injection
463 water (100 μL). At-211 aqueous solution (63 MBq, 50 μL) was mixed with 1% ascorbic acid,
464 2.3% MEYLON Injection aqueous solution (1 mL). After stirreing briefly, the reaction solution
465 of At-211 was left to stand for 1hour at room temperature under sealed condition to afford the
466 Na[At-211]. The Na[At-211] solution was dissolved 1% ascorbic acid, 2.3% MEYLON Injection
467 aqueous solution, and used animal experiments and the cell tracer experiments.
468

469 **Thin-Layer Chromatography (TLC) Analysis**

470 Thin-layer chromatography (TLC) was performed using silica gel 60 plates (Merck) as
471 the stationary phase. Samples (5 μL, 280 kBq) were spotted onto the plate and developed in a
472 solvent system consisting of acetonitrile and Milli-Q water (CH_3CN:MQ = 2:1, v/v).
473 After development, the chromatograms were analyzed using a TLC scanner (Scan-RAM;
474 LabLogic Systems Ltd.) equipped with a ZnS scintillation detector. Radioactivity on the TLC
475 plates was quantified using the manufacturer's analysis software.
476

477 **Quantitative measurement of At-211 uptake**

478 Na[At-211] (10 kBq) was added to the DPC and NIS DPC cell and incubated for 5
479 min, 30 min, and 1 h, respectively. After incubation, the medium was removed and the cells were

480 collected. The radioactivity of the samples was then measured with a γ-counter, and the counts

481 per minute (CPM) were calculated.

482

483 **Visualization of alpha-ray**

484 Alpha-particle track images were acquired with a CMOS sensor at 1-s exposure,

485 yielding 600 frames each for NIS-DPS and DPC cells. Image analysis was conducted in ImageJ

486 (v1.54f). For each frame, a fixed intensity threshold was applied, followed by morphological

487 operations to generate a binarized mask of suprathreshold regions. Each image was then

488 accumulated with its corresponding mask to isolate regions of interest surrounding the α-particle

489 tracks, and the resulting stacks were Z-projected to produce composite track images.

490

ACKNOWLEDGEMENTS

The radioisotope of At-211 was produced at the RI Beam Factory operated by the RIKEN Nishina Center and the CNS, University of Tokyo, Japan. The authors gratefully acknowledge Yousuke Kanayama, Nozomi Sato, Akihiro Nambu, Tomohiro Tomitsuka, Hiromichi Shimizu, Yudai Shigekawa, Sayantani Mitra, and Keiko Watanabe of RIKEN Nishina Center for technical assistance with the At-211 production.

FUNDING

This work was supported by Grants-in-Aid for Scientific Research (KAKENHI) from the Japan Society for the Promotion of Science (JSPS), including "Development of novel radiopharmaceuticals using α-emitting radionuclides and antibody drug delivery systems" (grant number 23H00419); "Collaborative research on therapeutic radionuclide production and radiopharmaceutical synthesis" (grant number 20KK0174); "Development of novel therapy for peritoneal dissemination using neoantigen activation induced by short-lived α-emitting radionuclides" (grant number 24K02393); "Experimental study of intraperitoneal radiotherapy for gastric cancer dissemination using highly selective short-lived α-particle delivery" (grant number 19H03510); and "Development of radiation imaging technology for detecting micro–peritoneal dissemination of gastric cancer" (grant number 21H00169).

Additional support was provided by the Uehara Memorial Foundation ("Development of radionuclide production technology and novel radiopharmaceuticals through accelerator science") and the Nakatani Foundation for Advancement of Measuring Technologies in Biomedical Engineering ("Development of theranostic technology using α-emitting radionuclides").

AUTHOR CONTRIBUTIONS

S.N. conceived and supervised the study and performed animal experiments. K.K., H.Y., H.M., T.Y., and W.-Y.D. conducted animal experiments. Y.W. performed α-particle therapy experiments and contributed to manuscript preparation. T.T. performed sodium astatide (At-211) synthesis. M.K. conducted cell culture experiments. A.T. performed RNA-seq data acquisition. T.Ta. analyzed pathological specimens. J.J. conducted At-211 compound analyses. Y.K. performed imaging studies. A.S. carried out α-particle uptake assays. R.N. prepared DPC cells. W.Y. performed functional analyses of DPCs. H.S. performed genetic modification of DPCs. K.I. managed DPC manufacturing and quality control. H.H. and X.Y. developed At-211 production technology. M.Yo. performed direct α-particle imaging. A.Yo. developed scintillators. T.K. and N.T. performed bioinformatics analyses. M.N. supervised bioinformatics and data integration. All authors discussed the results and approved the final manuscript.

COMPETING INTERESTS

N/A

DATA AND MATERIALS AVAILABILITY

under preparation

534 **REFERENCES**

535 A randomized, double-blind, placebo-controlled, multicenter study to evaluate the safety and
536 efficacy of JTR-161 in patients with acute ischemic stroke (jRCT1080224505).
537 **Japan Registry of Clinical Trials**, registered in 2022.
538

539 C. Nito, K. Sowa, M. Nakajima, Y. Sakamoto, S. Suda, Y. Nishiyama, A. Nakamura-Takahashi,
540 Y. Nitahara-Kasahara, M. Ueda, T. Okada, and K. Kimura, Transplantation of human dental pulp
541 stem cells ameliorates brain damage following acute cerebral ischemia. **Biomedicine &**
542 **Pharmacotherapy** 108, 1005–1014 (2018).
543

544 S. Gronthos, M. Mankani, J. Brahim, P. G. Robey, and S. Shi, Postnatal human dental pulp stem
545 cells (DPSCs) in vitro and in vivo. **Proceedings of the National Academy of Sciences of the**
546 **United States of America** 97, 13625–13630 (2000).
547

548 Y. Yamamoto, S. Nomura, A. Hosoi, K. Nagaoka, T. Iino, T. Yasuda, T. Saito, H. Matsushita, E.
549 Uchida, Y. Seto, J. R. Goldenring, K. Kakimi, M. Tatematsu, and T. Tsukamoto, Established
550 gastric cancer cell lines transplantable into C57BL/6 mice show fibroblast growth factor receptor
551 4 promotion of tumor growth. **Cancer Science** 109(5), 1480–1492 (2018).

K. Nagaoka, H. Nakanishi, H. Tanaka, J. Anindita, T. Kawamura, T. Tanaka, T. Yamashita, A. Kuroda, S. Nomura, H. Akita, K. Itaka, T. Kodama, and K. Kakimi, Neoantigen mRNA vaccines induce progenitor-exhausted T cells that support anti-PD-1 therapy in gastric cancer with peritoneal metastasis. **Gastric Cancer** 28(5), 825–836 (2025).

E. Darrouzet, S. Lindenthal, D. Marcellin, J.-L. Pellequer, and T. Pourcher, The sodium/iodide symporter: state of the art of its molecular characterization. **Biochimica et Biophysica Acta** 1838(1 Pt B), 244–253 (2014).

T. Watabe, Y. Liu, K. Kaneda-Nakashima, T. Sato, Y. Shirakami, K. Ooe, A. Toyoshima, E. Shimosegawa, Y. Wang, H. Haba, T. Nakano, A. Shinohara, and J. Hatazawa, Comparison of the therapeutic effects of [211At]NaAt and [131I]NaI in an NIS-expressing thyroid cancer mouse model. **International Journal of Molecular Sciences 23**(16), 9434 (2022).

S. Yamamoto, M. Yoshino, K. Kamada, R. Yajima, A. Yoshikawa, K. Nakanishi, and J. Kataoka, Development of an ultrahigh-resolution real-time alpha-particle imaging system for observing the trajectories of alpha particles in a scintillator. **Scientific Reports** 13(1), 4955 (2023).

M. Yoshino, A. Sugiyama, T. Tatsumi, S. Nomura, S. Shimazoe, S. Yamamoto, A. Taguchi, T. Tanaka, M. Kobayashi, and Y. Wada, Observation of At-211 accumulated cells using a real-time alpha-particle imaging system. **RIKEN Accelerator Progress Report**, accepted (2025).

L. Jiang, Y.-Q. Zhu, R. Du, Y.-X. Gu, L. Xia, F. Qin, and H. H. Ritchie, The expression and role of stromal cell–derived factor-1α–CXCR4 axis in human dental pulp. **Journal of Endodontics** 34(8), 939–944 (2008).

S. Yamaguchi, R. Shibata, N. Yamamoto, M. Nishikawa, H. Hibi, T. Tanigawa, M. Ueda, T. Murohara, and A. Yamamoto, Dental pulp–derived stem cell conditioned medium reduces cardiac injury following ischemia–reperfusion. **Scientific Reports** 5, 16295 (2015).

M. Li, X. Sun, L. Ma, L. Jin, W. Zhang, M. Xiao, and Q. Yu, SDF-1/CXCR4 axis induces human dental pulp stem cell migration through FAK/PI3K/Akt and GSK3β/β-catenin pathways. **Scientific Reports** 7, 40161 (2017).

V. C. M. Neves, V. Yianni, and P. T. Sharpe, Macrophage modulation of dental pulp stem cell

activity during tertiary dentinogenesis. **Scientific Reports** 10(1), 20216 (2020).

C. Kornsuthisopon, A. Chansaenroj, J. Manokawinchoke, K. A. Tompkins, N. Pirarat, and T. Osathanon, Non-canonical Wnt signaling participates in Jagged1-induced osteo/odontogenic differentiation in human dental pulp stem cells. **Scientific Reports** 12(1), 7583 (2022).

M. Irfan and S. Chung, C5L2 modulates BDNF production in human dental pulp stem cells via the p38α pathway. **Scientific Reports** 13(1), 74 (2023).

S. Suda, C. Nito, M. Ihara, Y. Iguchi, T. Urabe, Y. Matsumaru, N. Sakai, and K. Kimura; J-REPAIR Trial Group, Randomised placebo-controlled multicentre trial to evaluate the efficacy and safety of JTR-161, allogeneic human dental pulp stem cells, in patients with acute ischaemic stroke (J-REPAIR). **BMJ Open 12**(5), e054269 (2022).

X. Yin, N. Sato, A. Nambu, Y. Shigekawa, and H. Haba, Progress of 211At production at the RIKEN AVF cyclotron. **RIKEN Accelerator Progress Report** 56, 151 (2023).

X. Yin, N. Sato, A. Nambu, Y. Kanayama, Y. Shigekawa, and H. Haba, Modification of 211At

production apparatus to increase its production efficiency. **RIKEN Accelerator Progress Report** 57, 149 (2024).

611 **FIGURE LEGENDS**

612 **Figure 1. Isolation and characterization of dental pulp–derived stem cells (DPCs).**

613 (a) The dental pulp is a soft connective tissue located within the interior of the tooth.

614 (b) After extraction of the dental pulp tissue, the connective components were enzymatically

615 digested, mechanically minced with a sharp blade, and cultured in growth medium supplemented

616 with differentiation inhibitors. Proliferating cells were isolated and purified as dental pulp–

617 derived stem cells (DPCs).

618 (c) Colony-forming assay of DPCs. HeLa cells were used as a control. Cells were stained with a

619 fluorescent dye and cultured for 0 or 7 days. Fluorescence intensity was quantified as relative

620 fluorescence units (RFU; n = 3). Representative microscopic images of colonies are shown. Scale

621 bar, 10 μm.

622

623 **Figure 2. Confirmation of DPC accumulation in peritoneal tumor tissue.**

624 (a–d) Macroscopic and fluorescence imaging analyses of a gastric cancer peritoneal dissemination

625 model after intraperitoneal administration of DiR-labeled dental pulp–derived stem cells (DPCs).

626 Panels (a) and (b) show macroscopic views of the peritoneal serosa, where blue lines outline the

627 regions of peritoneal tumor nodules. Corresponding in vivo imaging system (IVIS) fluorescence

628 images (c and d) demonstrate colocalization of fluorescence signals with the tumor lesions

629 identified in (a) and (b).

630 (e–g) Histological observation of peritoneal tumor tissue 1.5 weeks after intraperitoneal

631 administration of DPCs. Nuclei were counterstained with hematoxylin and eosin stain, and DPCs

632 were detected by immunostaining using an anti-human Lamin B1 antibody followed by an HRP-

633 conjugated secondary antibody. Panel (e) shows a low-magnification image, and (f) shows a high-

634 magnification view of the region. Arrows indicate DPCs accumulated within peritoneal tumor

635 lesions. Panel (g) shows tissue from a normal mouse injected with DPCs as a control.

636 (h) Migration assay evaluating DPC chemotaxis toward YTN16 gastric cancer cells. The lower

637 chamber contained 5×10^4 to 2×10^5 YTN16 cells, and 1×10^5 DiR-labeled DPCs were seeded

638 in the upper chamber. After 48 hours, fluorescence intensity of migrated cells was quantified.

639 DPC migration increased in proportion to the number of YTN16 cells in the lower chamber ($n =$

640 10; $p < 0.001$).

641

642 **Figure 3. Functional transduction of the sodium/iodide symporter (NIS) into dental pulp–**

643 **derived stem cells (DPCs).**

644 (a) Gene expression levels of parental DPCs and sodium/iodide symporter (NIS)–transduced

645 DPCs (NIS-DPCs) quantified from RNA-seq data and presented as transcripts per million (TPM)

646 values. Among iodide symporter genes, SLC5A5 was transduced and expressed in NIS-DPC.

GAPDH and beta-actin (ACTB) were controls.

(b) Comparison of iodide uptake between DPCs and NIS-DPCs. Data for NIS-DPCs were obtained from three independent donors.

(c) Correlation analysis between NIS-positive cell fraction and iodide uptake levels in NIS-DPCs.

(d) In vivo localization of NIS-DPCs within tumor tissue, showing accumulation comparable to that of unmodified DPCs.

(e) Migration assay using Transwell chambers with YTN16 gastric cancer cells placed in the lower compartment. NIS-DPCs exhibited cell number–dependent migration similar to DPCs ($n = 10$; $p < 0.01$).

Figure 4. Preparation and functional characterization of sodium astatide-211 (Na[At-211]) and its uptake by NIS-DPCs.

(a) Reaction protocol for converting purified free astatine-211 (At-211), produced at an accelerator facility, into a homogeneous sodium astatide form (Na[At-211]). The free isotope can exist in multiple chemical species, and sodium conjugation was performed to stabilize its form.

(b) Thin-layer chromatography (TLC) analysis of At-211 before and after sodium conjugation. Left: TLC profile of free At-211 (~100 kBq). Right: TLC profile of Na[At-211] (~280 kBq). Arrows indicate the Na[At-211] peak position.

665 (c) Cellular uptake of Na[At-211] by dental pulp–derived stem cells (DPCs) and NIS-expressing

666 DPCs (NIS-DPCs). DPCs or NIS-DPCs (5×10^4 cells per well) were seeded in 24-well plates and

667 incubated with 10 kBq Na[At-211]. At 5, 10, and 60 min, cells were collected, fractionated, and

668 measured for protein concentration and radioactivity. Radioactivity normalized to protein content

669 was calculated. NIS-DPCs exhibited approximately tenfold higher At-211 uptake than parental

670 DPCs (n = 3; black bars, DPCs; gray bars, NIS-DPCs).

671

672 **Figure 5. Detection of α-particle emission from NIS-transduced dental pulp–derived stem**

673 **cells (NIS-DPCs).**

674 (a) Schematic diagram of the α-particle detection system. α-particles emitted from cells (left) are

675 first converted into photons by a GAGG:Ce scintillator. The photons are then amplified and

676 reflected within the detector and captured by a cooled CMOS sensor positioned at the top.

677 (b) Overview of the α-particle detection device.

678 (c–d) NIS-DPCs (1×10^4 cells per well) were seeded in 8-well chamber slides and incubated for

679 30 min with 500 kBq of sodium astatide–211 (Na[At-211]). Cells were then fixed with formalin

680 and imaged. Arrowheads indicate the localization of individual cells.

681 (f–h) DPCs (1×10^4 cells per well) were similarly treated with 500 kBq Na[At-211], incubated

682 for 30 min, fixed with formalin, and imaged. Arrowheads indicate cell localization.

683 (c and f) Optical microscopic images of cells. (d and g) Corresponding α-camera signal images.

684 (e and h) Merged images combining optical and α-particle signals. Scale bar, 100 μm.

685

686 **Figure 6. Therapeutic efficacy of NIS-DPCs combined with At-211 in a murine gastric**

687 **cancer peritoneal dissemination model.**

688 C57BL/6 mice were inoculated intraperitoneally with 1×10^7 YTN16 gastric cancer cells to

689 establish a peritoneal dissemination model. One week later, 0.5×10^6 NIS-DPCs were

690 intraperitoneally administered every other day for three doses. Three days after the final cell

691 transplantation, 0.6 MBq of sodium astatide-211 (Na[At-211]) was injected intraperitoneally, and

692 mice were sacrificed 1.5 weeks later for macroscopic observation.

693 (a) Untreated control group.

694 (b–d) Mice receiving one, two, or three intraperitoneal administrations of NIS-DPCs followed by

695 Na[At-211], respectively. Peritoneal tumor burden decreased in proportion to the number of NIS-

696 DPC treatments.

697 (e) Macroscopic scoring of peritoneal dissemination was performed on a 0–4 scale.

698 (f) Quantitative comparison of macroscopic scores among the untreated group, Na[At-211]-only

699 group, and the group receiving three NIS-DPC administrations plus Na[At-211]. Statistical

700 analysis was performed using Tukey's test ($n = 10$; $p < 0.01$, $*p < 0.001$).

701 (g) Kaplan–Meier survival analysis after one month following Na[At-211] administration. Mice

702 treated with three doses of NIS-DPCs plus Na[At-211] (#3) showed a significant survival

703 advantage compared with the untreated group (#1) and the Na[At-211]-only group (#2). Control

704 groups without YTN16 cell implantation included Na[At-211]-only (#5) and NIS-DPC × 3 +

705 Na[At-211] (#6) treatments (n = Y; p <○○, *p < ○○).

706

707 **Figure 7. Graphical Summary. Stepwise overview of the NIS-DPC cancer-targeting concept.**

708 The schematic illustrates the translational workflow of sodium/iodide symporter (NIS)–

709 expressing dental pulp–derived stem cells (NIS-DPCs) as a targeted theranostic platform for

710 cancer therapy.

711 Step 1 (engineering). Dental pulp–derived stem cells were genetically modified to express the

712 sodium/iodide symporter (NIS), which mediates the cellular uptake of both iodide and astatine.

713 The lower panel depicts this dual transport function of NIS, highlighting its ability to internalize

714 iodide and the α-emitting radionuclide At-211.

715 Step 2 (targeting and accumulation). Following administration, NIS-DPCs preferentially

716 accumulated in cancer cells, enabling the selective delivery of At-211 to tumor sites.

717 Step 3 (localized therapy/outcome). Localized α radiation at the tumor site induced targeted

718 cytotoxicity, demonstrating the translational potential of NIS-DPC–mediated therapy for precise

719 cancer treatment.

720

Fig.1a&b

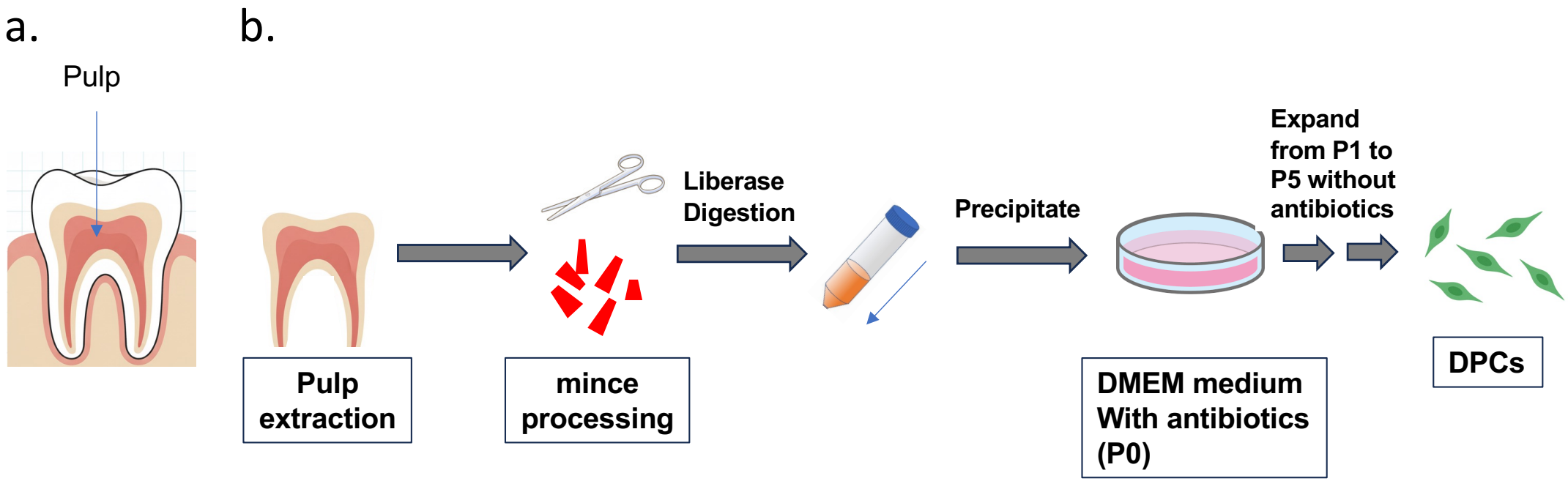
a.
Pulp
b.
Pulp extraction
mince processing
Liberase Digestion
Precipitate
DMEM medium With antibiotics (P0)
Expand from P1 to P5 without antibiotics
DPCs

Fig.1c

c.

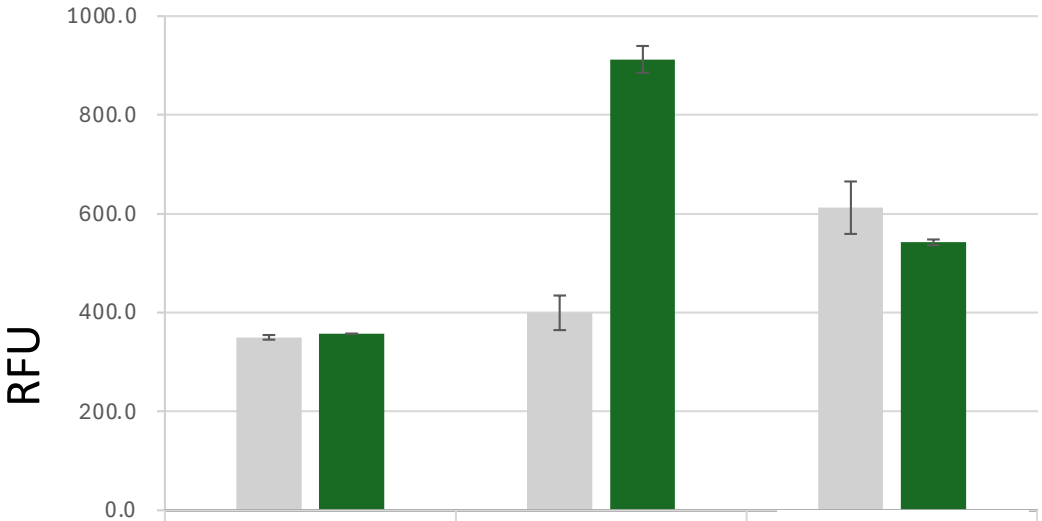

	Culture Medium	Hela	DPC (DC1751)
Day0	350.1	399.7	612.4
Day7	357.2	912.5	542.3

【Day0】

【Day7】

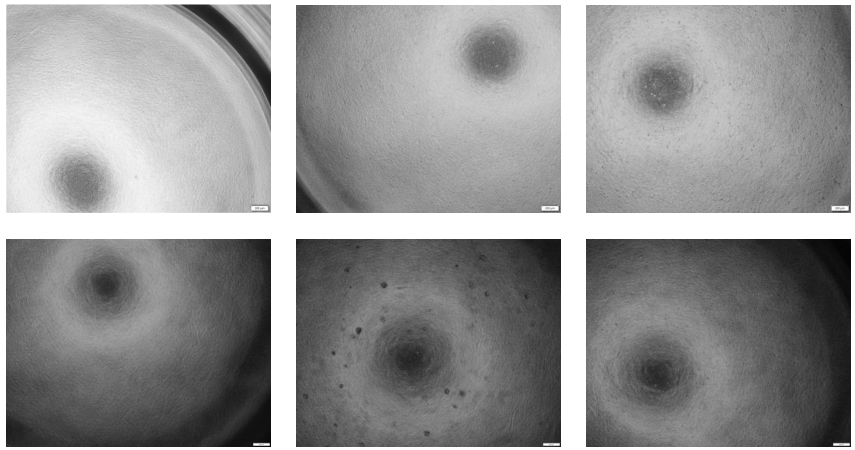

Fig.2a~d

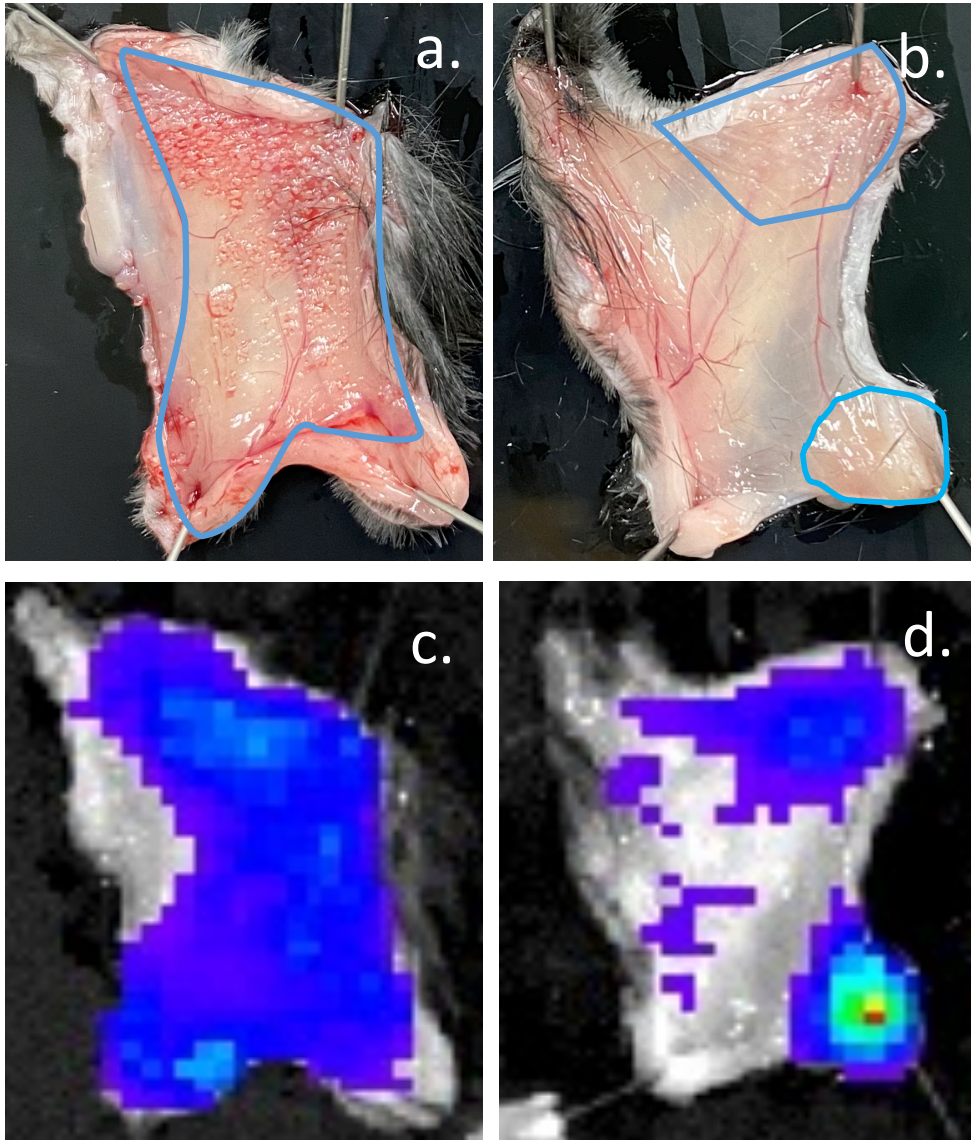

Fig. 2e~g

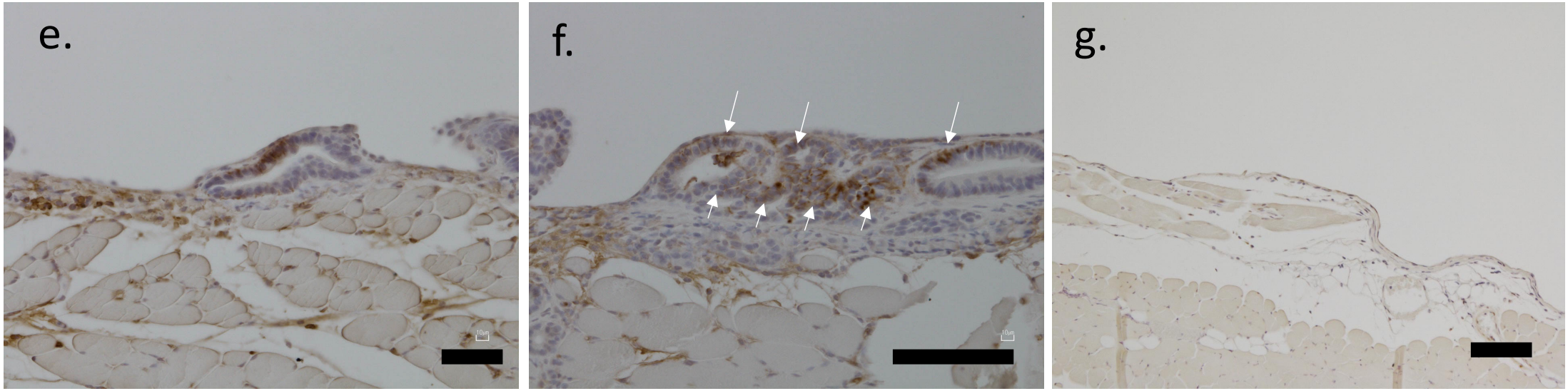

Fig. 2h

h.

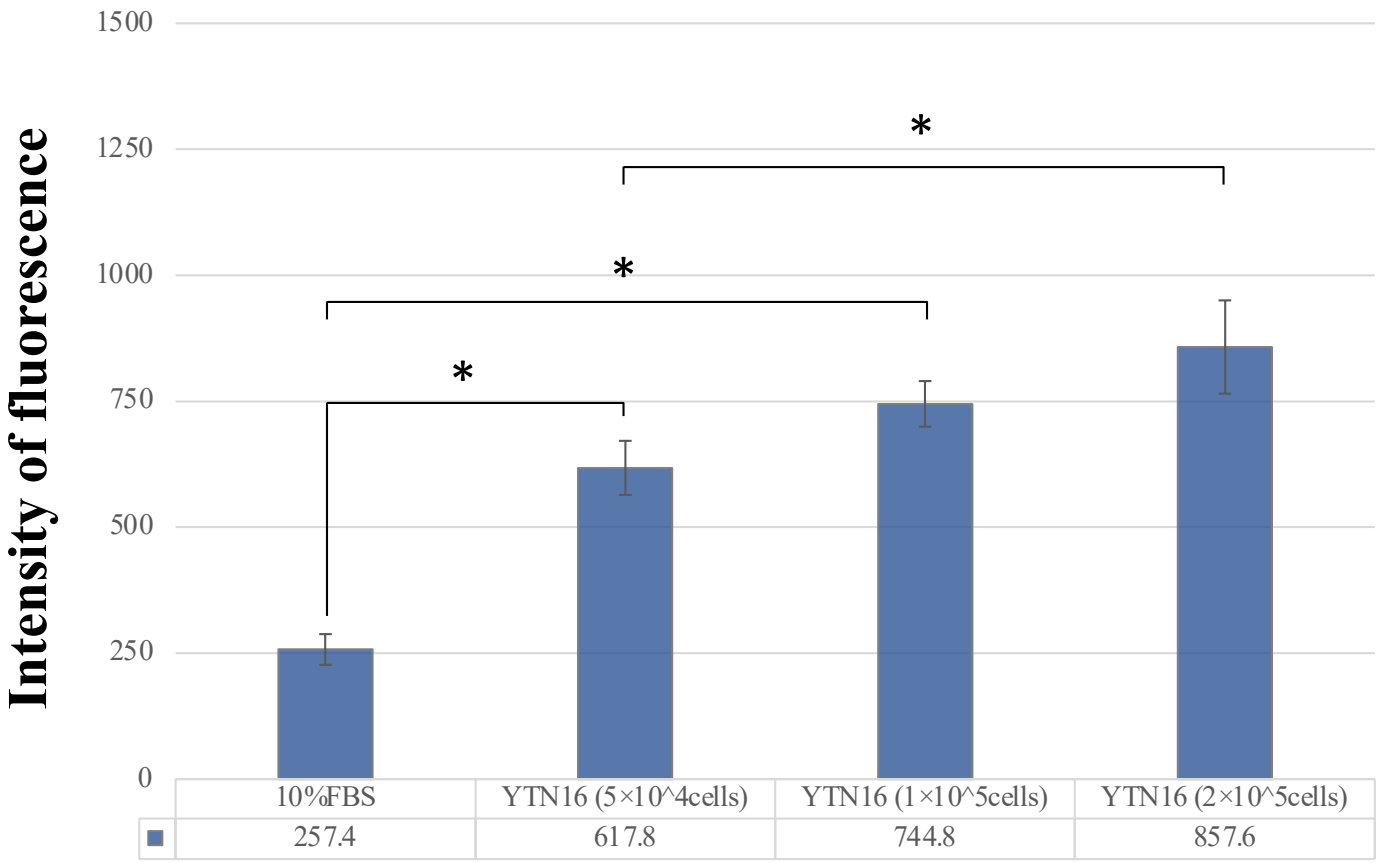
Intensity of fluorescence
1500
1250
1000
750
500
250
0
*
*
*
10%FBS
YTN16 (5×10^4cells)
YTN16 (1×10^5cells)
YTN16 (2×10^5cells)
257.4
617.8
744.8
857.6

Fig. 3a

a.

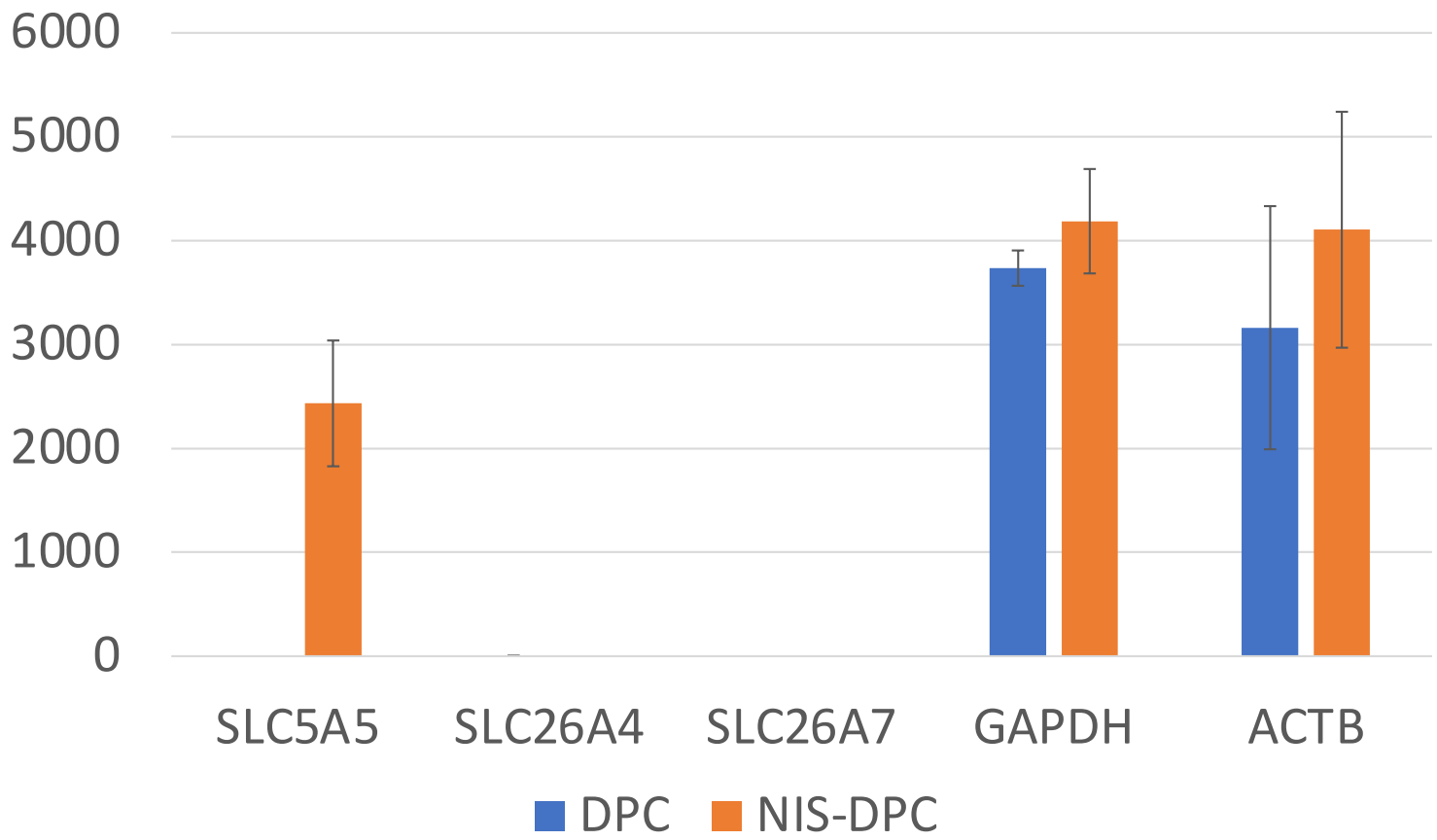
6000
5000
4000
3000
2000
1000
0
SLC5A5
SLC26A4
SLC26A7
GAPDH
ACTB
DPC
NIS-DPC

Fig.3b&c

b.

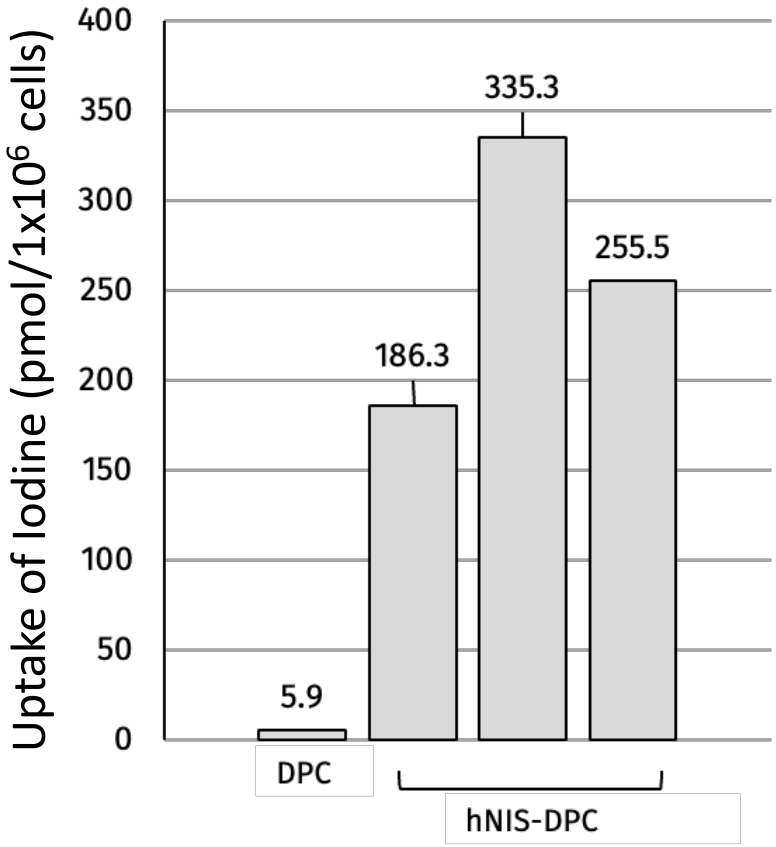
Uptake of Iodine (pmol/1x10^6 cells)
400
350
300
250
200
150
100
50
0
5.9
186.3
335.3
255.5
DPC
hNIS-DPC

c.

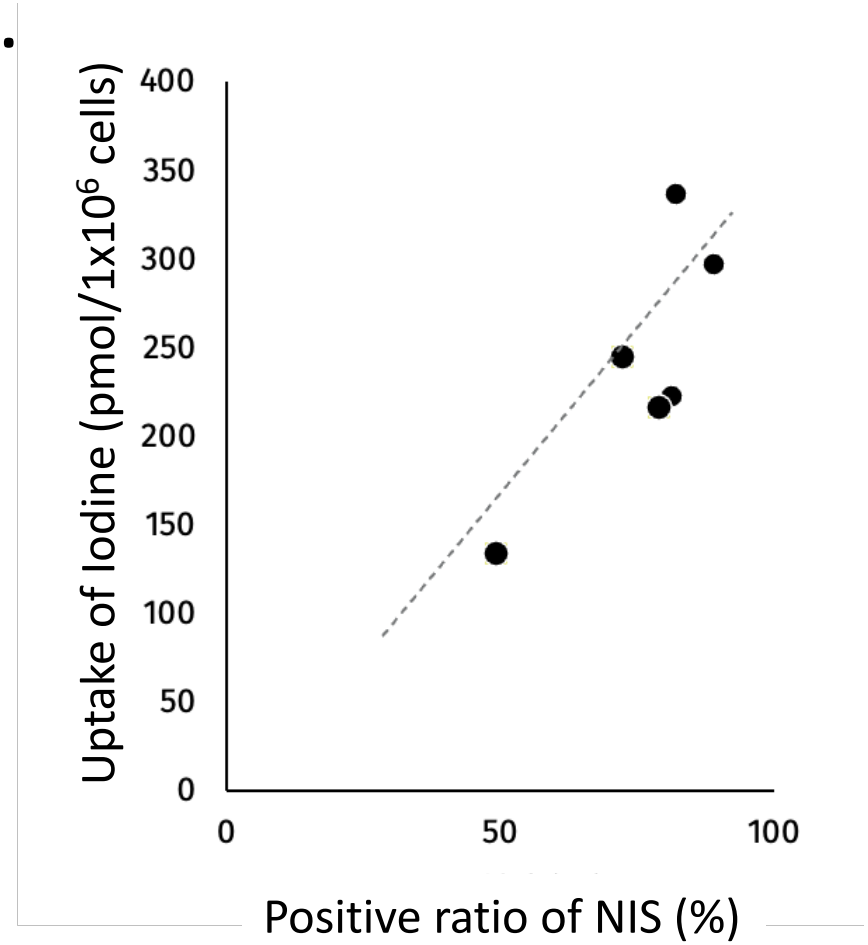
Uptake of Iodine (pmol/1x10^6 cells)
400
350
300
250
200
150
100
50
0
0
50
100
Positive ratio of NIS (%)

Fig.3d, e, f

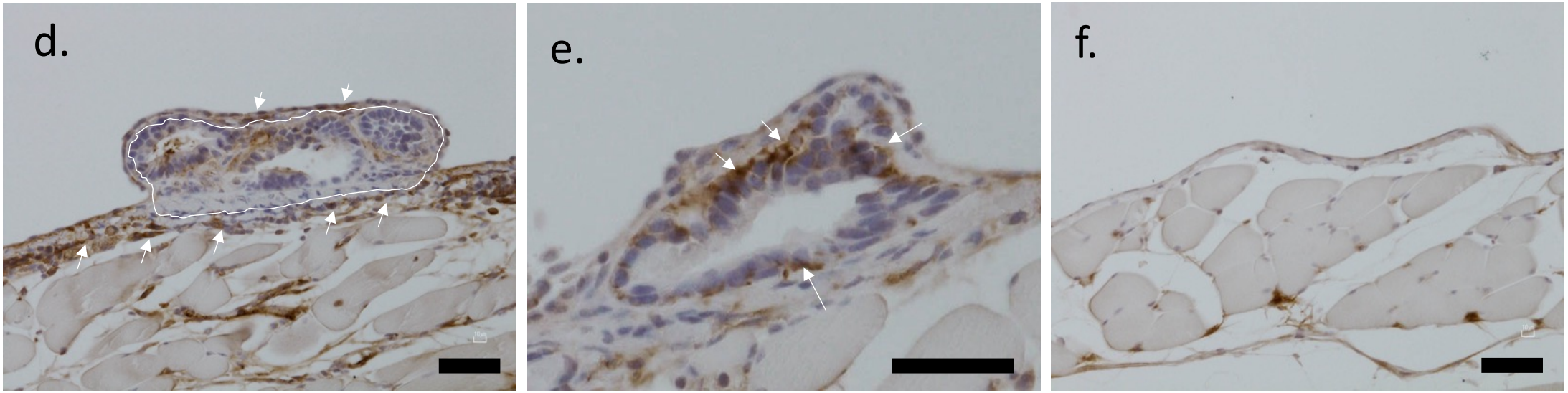

Fig.3g

g.

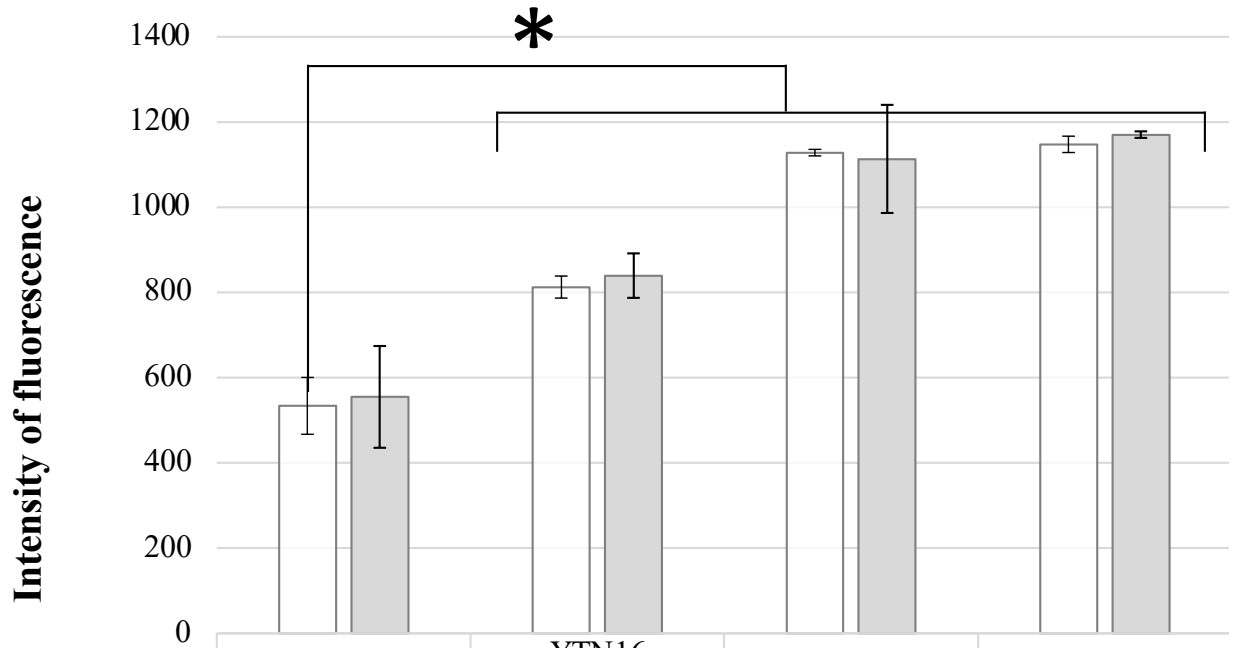

	10%FBS	YTN16 (2.5×10^4cells)	YTN16 (1×10^5cells)	YTN16 (4×10^5cells)
□DPC P10	533.9	812.8	1128.2	1147.7
▨NIS-DPC P10	555.0	839.6	1113.5	1170.5

Fig. 4a&b

a.

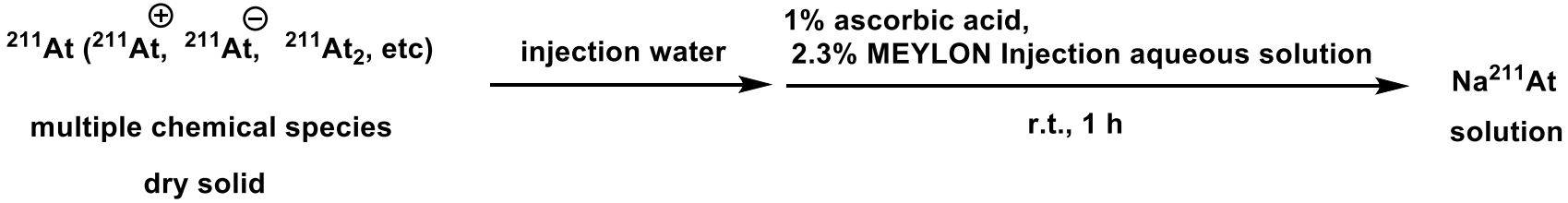
^{211}At ($^{211}At^{\oplus}$, $^{211}At^{\ominus}$, $^{211}At_2$, etc)
multiple chemical species
dry solid
injection water
1% ascorbic acid,
2.3% MEYLON Injection aqueous solution
r.t., 1 h
$Na^{211}At$
solution

b.

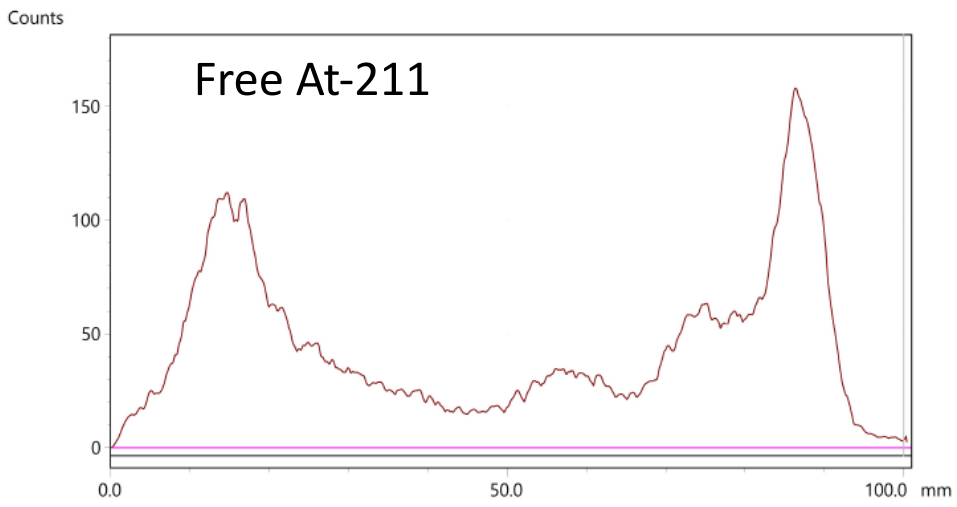
Counts
Free At-211
150
100
50
0
0.0
50.0
100.0
mm

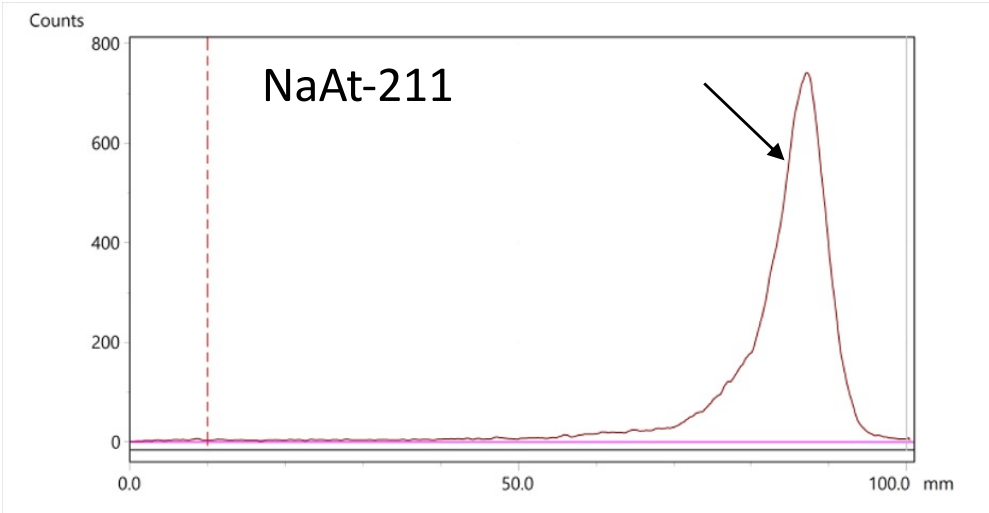
Counts
NaAt-211
800
600
400
200
0
0.0
50.0
100.0
mm

Fig. 4c

c.

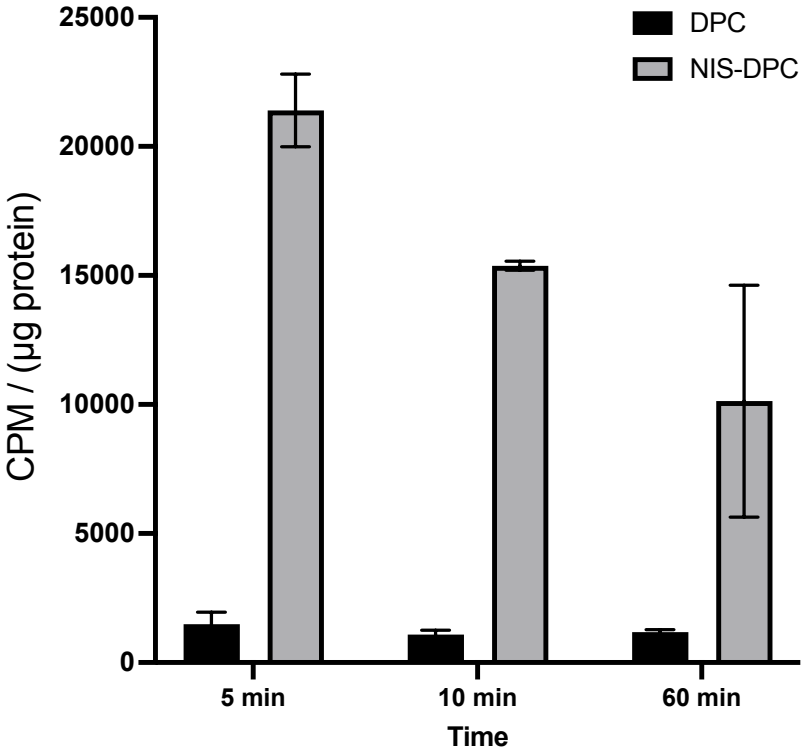
DPC
NIS-DPC
25000
20000
15000
10000
5000
0
CPM / (µg protein)
5 min
10 min
60 min
Time

Fig. 5

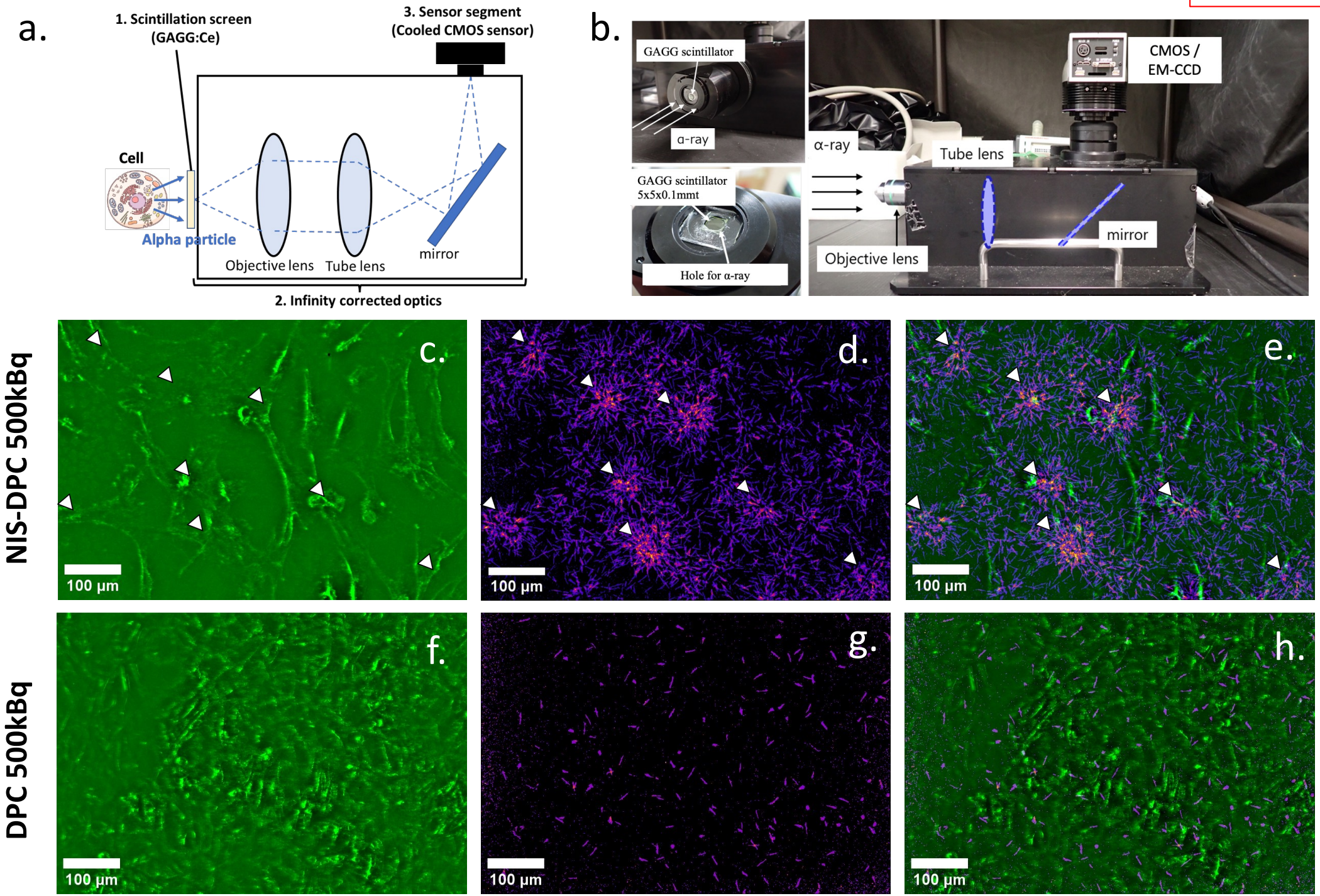
a.
1. Scintillation screen
(GAGG:Ce)
3. Sensor segment
(Cooled CMOS sensor)
Cell
Alpha particle
Objective lens
Tube lens
mirror
2. Infinity corrected optics
b.
GAGG scintillator
α-ray
GAGG scintillator
5x5x0.1mmt
Hole for α-ray
CMOS /
EM-CCD
α-ray
Tube lens
mirror
Objective lens
NIS-DPC 500kBq
DPC 500kBq
c.
d.
e.
f.
g.
h.
100 μm

Fig.6a~d

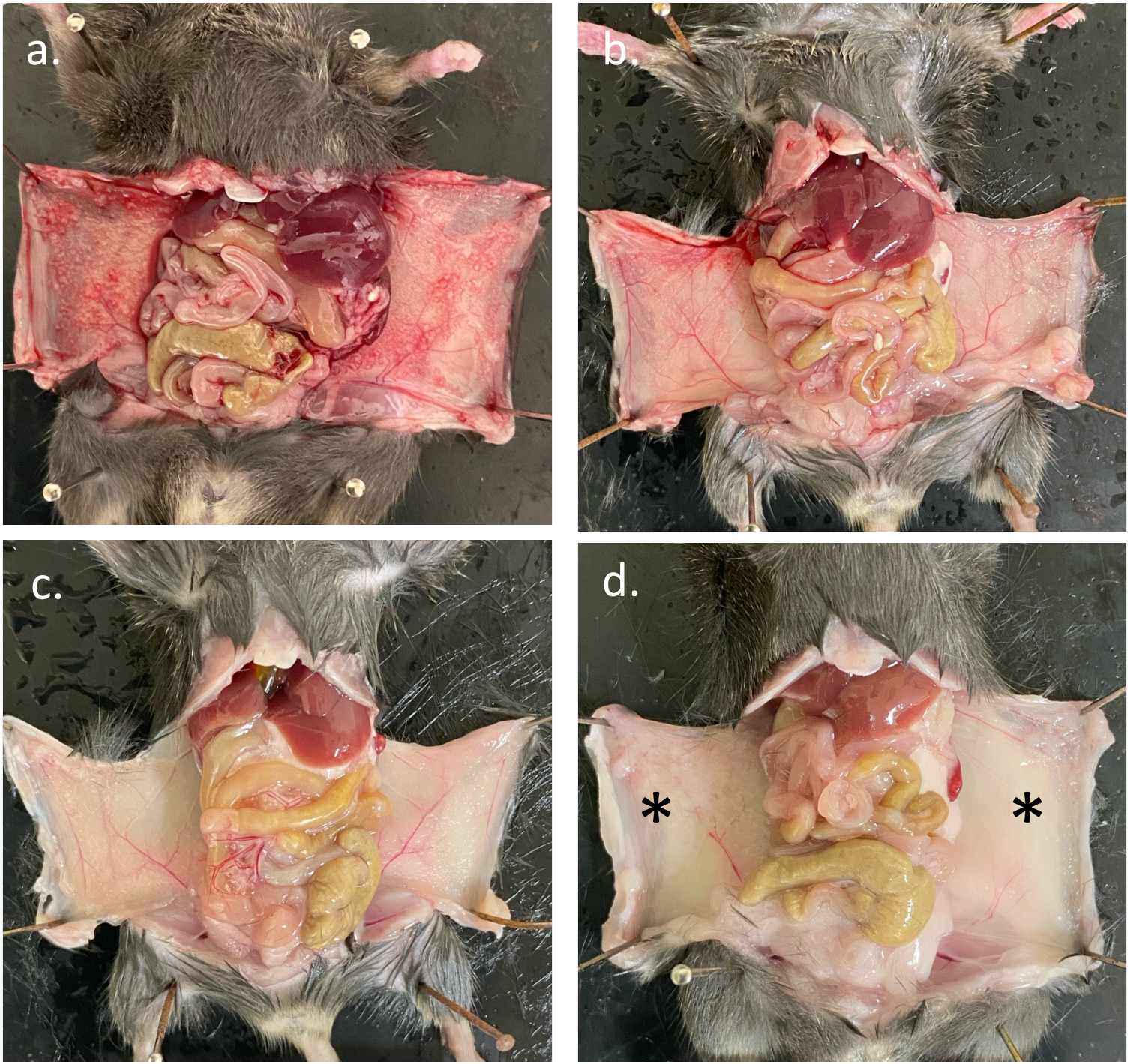

Fig.6e&f

e.

Macroscopic Score Evaluation of Peritoneal Tissue by Gross Examination
Rating scale: 0 (lowest) to 4 (highest)

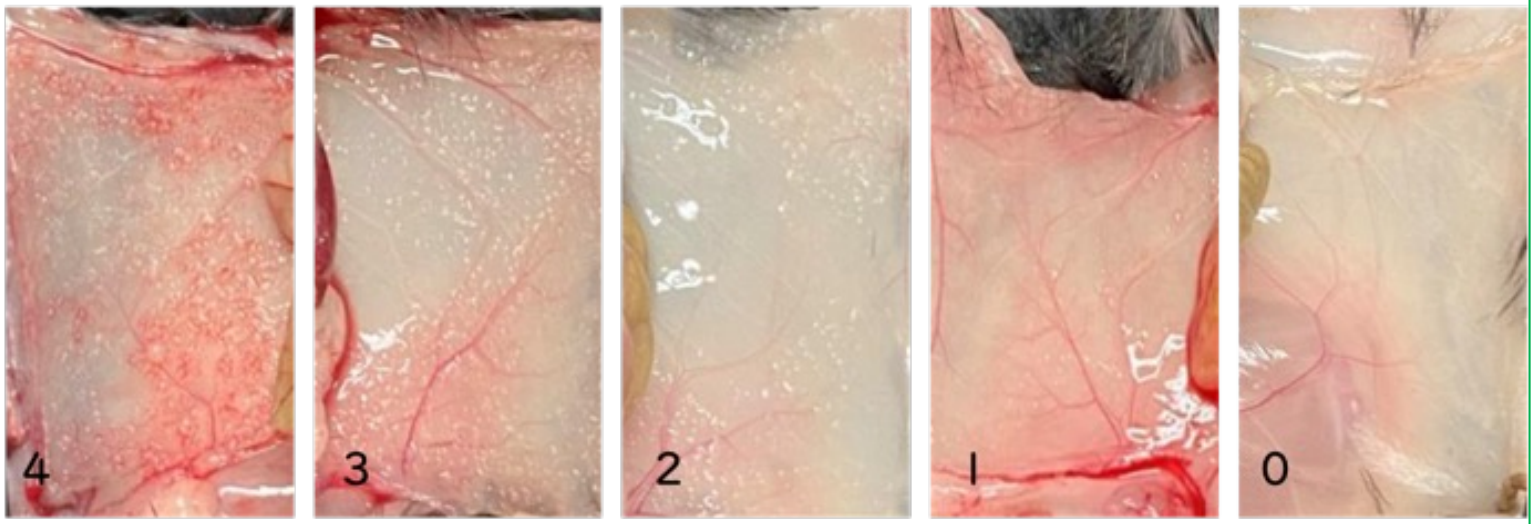

4	3	2	1	0
The grains are large and uniform throughout.	There are some grains, but not all over.	Clearly present, but the grains are small and watery.	Upon closer inspection, it exists only faintly.	No tumor

f.

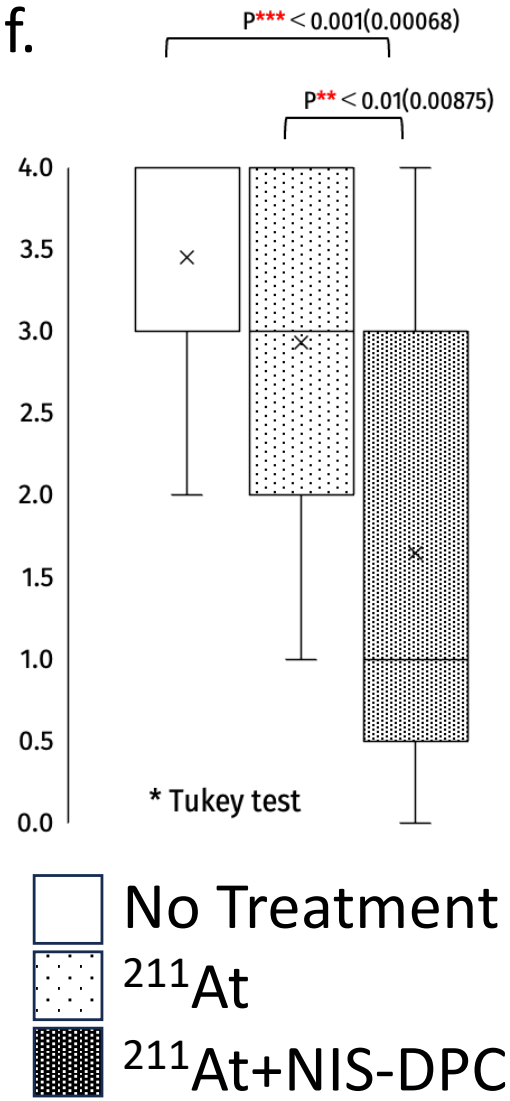

Fig.6g

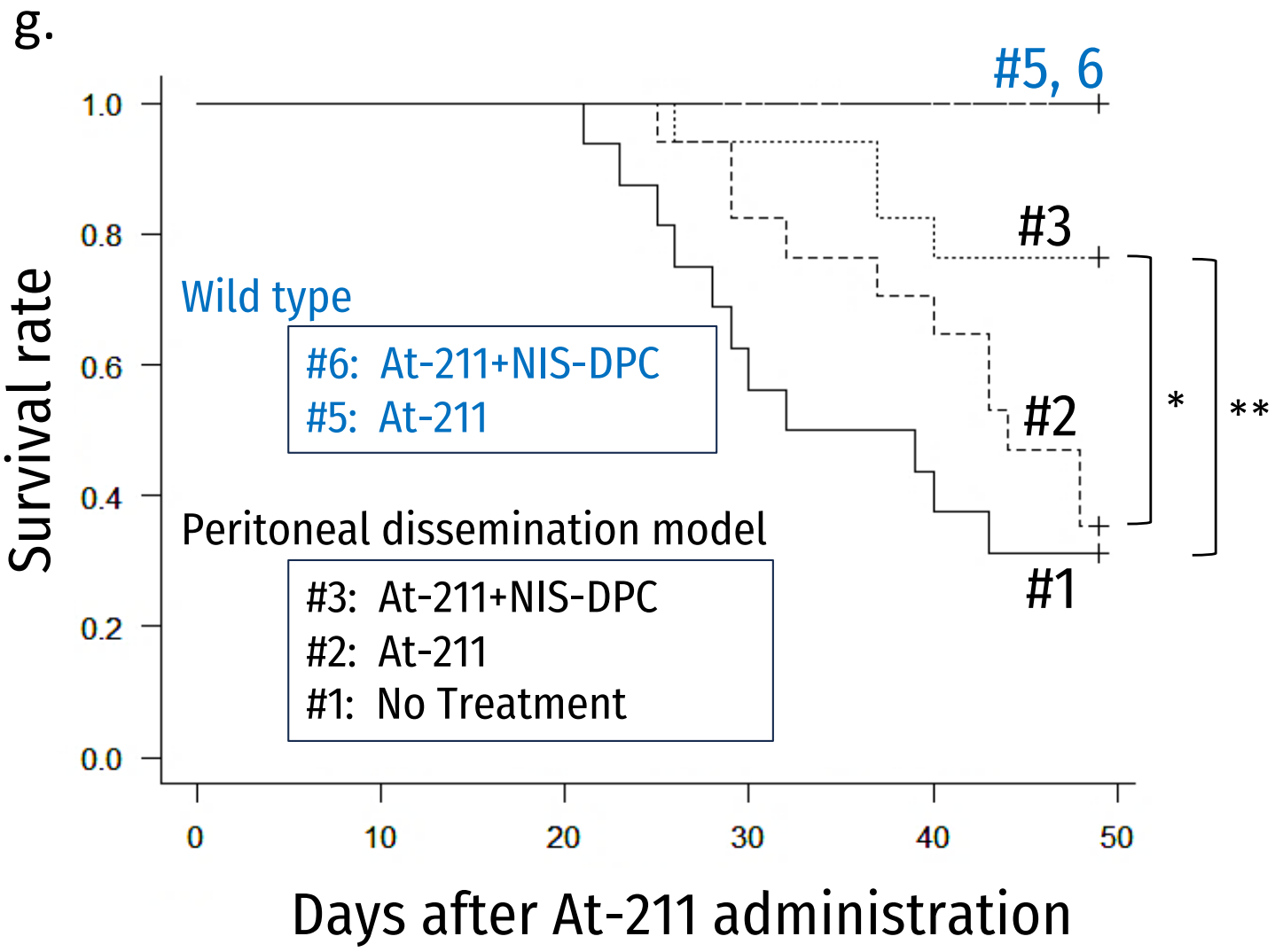
g.
#5, 6
#3
#2
#1
*
**
Wild type
#6: At-211+NIS-DPC
#5: At-211
Peritoneal dissemination model
#3: At-211+NIS-DPC
#2: At-211
#1: No Treatment
Survival rate
1.0
0.8
0.6
0.4
0.2
0.0
0
10
20
30
40
50
Days after At-211 administration

Fig. 7

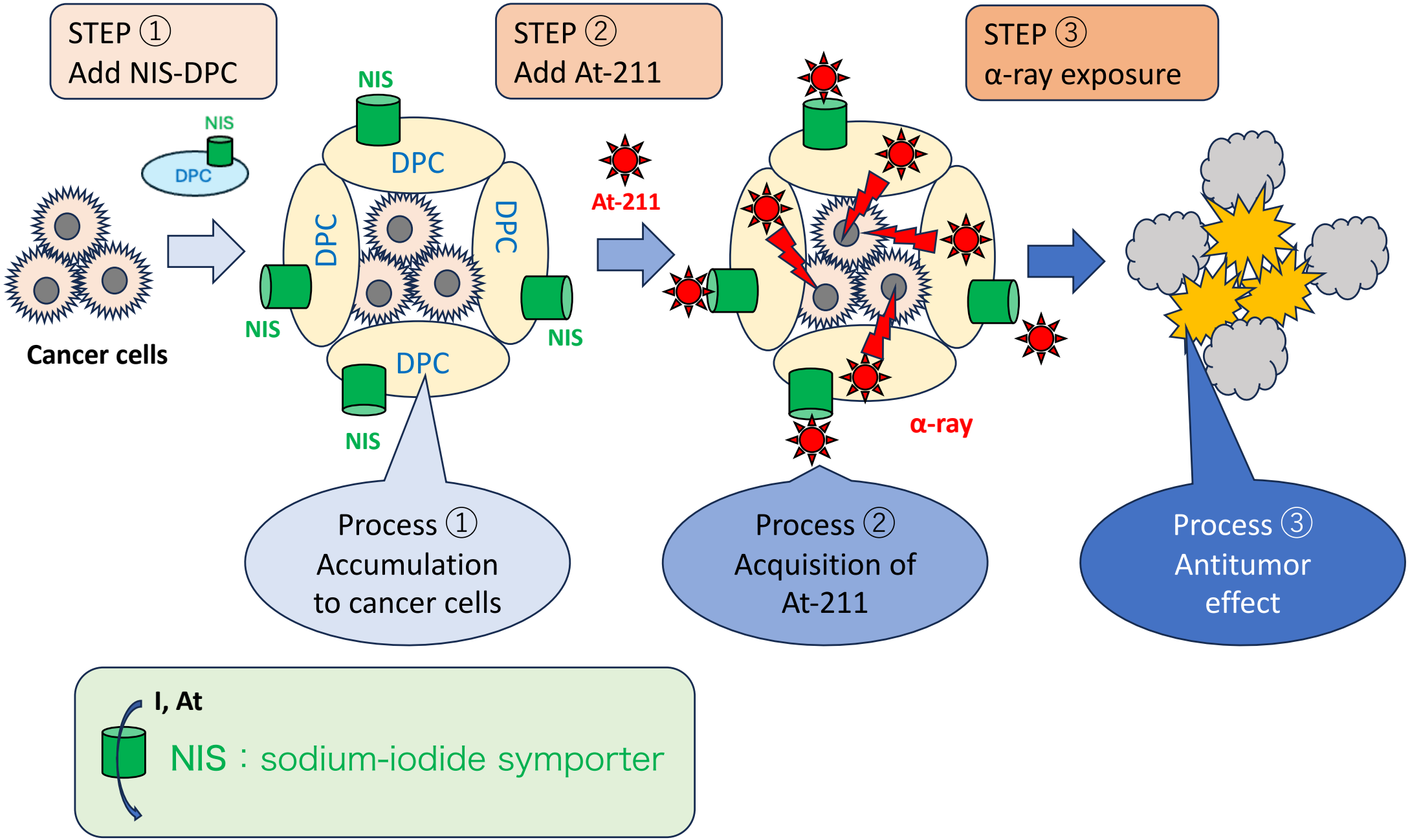
STEP ①
Add NIS-DPC
STEP ②
Add At-211
STEP ③
α-ray exposure
NIS
DPC
Cancer cells
At-211
α-ray
Process ①
Accumulation
to cancer cells
Process ②
Acquisition of
At-211
Process ③
Antitumor
effect
I, At
NIS : sodium-iodide symporter